HORIZON EUROPE PROGRAMME

TOPIC HORIZON-CL4-2022-RESILIENCE-01-24

GA No. 101091572

Graphene, MXene and ionic liquid-based sustainable supercapacitor

GREENCAP - Deliverable report

D2.3. - Electrochemical characterization of electrode/electrolyte interfaces

Funded by the European Union

Deliverable No.	GREENCAP D2.3	
Related WP	WP 2	
Deliverable Title	Electrochemical characterization of electrode/electrolyte interfaces	
Deliverable Date	2025-06-30	
Deliverable Type	REPORT	
Dissemination level	Public (PU)	
Author(s)	Prof. Andrea Balducci (FSU Jena)	
Checked by	Artur Ciesielski (UNISTRA)	2025-06-21
Reviewed by (if applicable)	Valeria Nicolosi (TCD) Tobias Burton, Sebastien Fantini & Alix Ladam (SOLV)	2025-06-22 2025-06-25
Approved by	Francesco Bonaccorso (BED) - Project coordinator	2025-06-25
Status	Final Draft	2025-06-25

Project summary

The GREENCAP project is dedicated to developing high-performance and sustainable cylindrical supercapacitors (SCs) by harnessing cutting-edge materials and principles of green chemistry. Its main objectives include:

- Design supercapacitors with superior performance and sustainability, pushing the boundaries of current energy storage technologies.
- Develop scalable prototypes that are ready for industrial manufacturing, ensuring the technology is viable for widespread application.
- Utilise layered two-dimensional materials (L2DMs): By incorporating these materials, GREENCAP aims to improve the energy storage capacity and overall efficiency of the supercapacitors.
- Employing ionic liquids (ILs): ILs based electrolytes offers wide electrochemical potential window, low volatility, and thermally stability alternative to conventional electrolytes, boosting both sustainability and performance of the SCs.

With considering these major objectives, GREENCAP aims to meet the increasing demand for energy storage solutions that are not only powerful and reliable but also sustainable. The project envisions applications across critical sectors such as clean transportation, renewable energy systems, and portable electronics.

Publishable summary

This deliverable presents a comprehensive electrochemical characterization of the electrode/electrolyte interface, carried out using a range of electroanalytical techniques such as cyclic voltammetry (CV), galvanostatic cycling with potential limitation (GCPL), and electrochemical impedance spectroscopy (EIS) and so on. A selection of critical raw material (CRM)-free layered two-dimensional materials (L2DMs), particularly MXene and curved graphene (CG) was chosen as electrode materials (EMs).

In this study, both protonated and aprotic ionic liquids (ILs) were developed, and their physicochemical properties were systematically investigated across a range of temperatures. Electrochemical performances were evaluated for these EMs in both protonated and aprotic ILs, first using half-cell configurations and later in full-cell assemblies.

As per electrochemical performance data provided by project partners for supercapacitors using CG and MXene electrodes, 1M $N_{1113}FSI$ in ACN, 1M $Pyr_{11}BF_4$ in ACN and $Pyr_{13}BF4$ in ACN have been selected for upscaling. These electrolytes are now being produced at the kilogram scale to support the development of first-generation prototypes.

Contents

Abbreviations

Abbreviation	Explanation
CG	Curved graphene
AC	Activated carbon
ILs	Ionic liquids
GCD	Galvanostatic charge-discharge
EDLCs	Electric double-layer capacitors
SC	Supercapacitor
CV	Cyclic voltammetry
GCPL	Galvanostatic cycling with potential limitation
EIS	Electrochemical impedance spectroscopy
L2DMs	Layered two-dimensional materials
CRM	Critical raw material
ACN	Acetonitrile
EMs	Electrode materials
Rct	Charge transfer resistance
Re	Electrolyte resistance
TGA	Thermogravimetric analysis

1 Introduction

Supercapacitors (SCs) are energy storage devices that store the charges through a physical process at the electrode-electrolyte interface. This enables SCs to deliver higher power, faster charge-discharge rates, and significantly greater cycle stability compared to conventional batteries, making them ideal for applications requiring rapid energy delivery and long operational lifetimes. However, SCs face key limitations, notably their low energy density (<10 Wh/kg) and restricted operating voltage window (<3.0 V) compared to batteries. Addressing these challenges requires the development of advanced electrode materials and electrolytes to improve energy storage capability while ensuring environmental sustainability and operational safety.

2D materials, such as graphene and MXene, are recognized as key candidates for supercapacitor EMs, due to their excellent electrical conductivity, high specific surface area, and tunable surface chemistry. Considering these advantages, work package 2 (WP2) is focused on enhancing the electrochemical performance of these materials through controlled surface functionalization and strategic hybridization. Additionally, WP2 aims to develop a fundamental understanding of electrode/electrolyte interface design and modelling, with the goal of identifying optimal material and electrolyte combinations that can significantly improve supercapacitor performance. This deliverable is specifically aligned with objective O2.3, which focuses on advancing the understanding of charge storage mechanisms at electrode/electrolyte interfaces. The EMs used to study this objective are developed under WP1.

Key achievements include:

- **Alternative sustainable EMs:** We found that curved graphene (CG) has emerged as a promising alternative to commercially used activated carbon for supercapacitor electrodes. Therefore, efforts were made to optimize and improve the production method of CG.
- **Synthesis of CRM-Free MXenes**: A variety of MXene materials have been successfully synthesized using both a mild etching method and a molten-salt approach. These methods enabled the production of high-quality MXenes with improved structural integrity.
- **Formulation of Aprotic ILs for EDLCs**: A selection of the highest-performing IL candidates has been identified to enhance the energy storage capacity of SCs.
- **Synthesis of Protonated ILs for MXenes:** Tailored protonated ILs were synthesized specifically for MXene-based electrodes. Protonated IL-based electrolyte formulations have shown promising performance, while more optimization and functionalization of MXenes is ongoing. This aims to improve the accessibility of electrolytes to MXene surfaces, enhancing electrochemical interactions and SC performance.

This deliverable describes the project efforts on the detail electrochemical characterization of electrode/electrolyte interface based on MXene and CG as SC electrode material (EMs) in both protic and aprotic ILs electrolytes.

2 Methods and core part of the report

2.1 Procedures for the synthesis of CRM-Free MXenes

At TCD, seven types of MAX phases were used: Ti_2AlC, Ti_3AlC_2 (both stoichiometric and Al-rich), Ti_3AlCN, Mo_2Ga_2C, Mo_2GaC, $(Mo_{2/3}Y_{1/3})_2AlC$, $Mo_2Ti_2AlC_3$

2.1.1 MXene synthesis by mild etching

If Al-rich MAX phase is used, first the excess aluminum must be washed away. This is achieved by stirring the MAX phase overnight in HCl (37%, Sigma) at a ratio of 1g MAX to 10 mL HCl. The mixture is then decanted into a 50 mL conical tube and centrifuged at 2800 g (5000 rpm) for 3 minutes. The clear supernatant is discarded, and the tube is refilled with deionized water. The centrifuging and discarding steps are repeated until the pH is ~6 (3-4 cycles is typical). The wet MAX phase powders are briefly dried by vacuum filtering to remove bulk liquids and then are dried in a 50 ˚C oven for ~30 m. It is not necessary that the MAX powders be completely dry before proceeding to the etching.

To etch the MAX phase, 20 mL of a 9M HCl solution is mixed with 1.6 g of LiF powder (Sigma) in a vented PTFE container and set in an oil bath, with stirring at 400 rpm until LiF is dissolved (~10 minutes). After that, 1 g of the MAX phase of choice (supplied by Carbon-Ukraine Ltd.) is added. To avoid excess heating, the MAX phase is added over approximately 5 minutes. The solution is then stirred at 400 rpm for 24 h at 35°C. After the etching is complete, the solution and solids are transferred to 250 mL conical tubes and filled with deionized water and centrifuged at 2800 g (5000 rpm) for 3 minutes. The clear supernatant is discarded, and the remaining sediment is dispersed again in deionized water and vortexed to ensure good suspension. The process is repeated until a pH > 6 is achieved.

To obtain mono- and few-layer flakes, the wet solids are resuspended in 50 mL of degassed deionized water in a 50 mL conical tube and sonicated for 1 h in an ice bath, then centrifuged for 30 minutes at 250 g (1500 rpm). The black supernatant of few- and single-layer flakes suspended in degassed deionized water is collected for further use. Typically, this supernatant is filtered on a Celgard 3501 microporous membrane to form freestanding films or is frozen and then freeze-dried. Large quantities of delaminated $Ti_3C_2T_x$ MXene have been produced by first freezing wet MXene solids, then thawing and using a high-capacity vortex mixer/shaker for 90 minutes at 2500 rpm followed by 30 min of centrifuge at 250 g (1500 rpm) for multiple (4-5) cycles. Up to 6 grams of freeze dried, delaminated MXene have been produced in this manner in a few days.

2.1.2 MXene synthesis by molten salt

MAX phase (Carbon Ukraine), LiCl (Sigma), LiF (Sigma), and $CuCl_2$ (Sigma) are measured in a 1:3:3:3 molar ratio (1:6:6:6 for Mo_2Ga_2C, due to the extra gallium stoichiometry). For small crucible, 0.5g of MAX phase is used, and for large crucible 1.0g of MAX phase is used. The powders are then mixed for approximately 10 minutes using a mortar and pestle to thoroughly combine and reduce particle size on the salts to create a uniform mixture. This mixture is then added to a crucible with lid and degassed by purging 3 times in the antechamber of an argon glove box. Finally, the crucible is transferred to a tube furnace and the tube furnace is sealed. Argon is allowed to purge the tube (450 sccm flow rate) for 1 hour. For the heating cycle, a ramp rate of 5 ˚C/min is used until the synthesis temperature of

700 ˚C is reached and held for 5 or more hours followed by allowing the furnace to cool to ambient temperature at its own rate. The synthesis temperatures, hold times, and molar ratio of MAX to salts are summarized in Table 1, below. Some MAX phases can also be etched by molten salt using bromide salts (NaBr, KBr, $CuBr_2$), also noted in the table below.

Table 1. Summary of synthesis conditions for molten salt synthesis of MXenes.

MAX phase	**Salt Ratio**	**Synthesis Temperature**	**Synthesis Time**
Ti_2AlC	1:3:3:3, Cl or Br Salts	700 ˚C	5 h
Ti_3AlC_2 (stoichiometric)	1:3:3:3, Cl or Br salts	700 ˚C	5 h
Ti_3AlCN	1:3:3:3, Cl or Br salts	700 ˚C	5 h
Mo_2Ga_2C	1:6:6:6, Cl or Br salts	700 ˚C	5 h
Mo_2GaC	1:3:3:3	700 ˚C	5 h
$Mo_2Ti_2AlC_3$	1:3:3:3	700 ˚C	5 h
$(Mo_{2/3}Y_{1/3})_2AlC$	1:3:3:3	700 ˚C	12h

After the furnace is cooled, the sample is removed, and the contents are transferred to 1-2 50 mL centrifuge tubes using deionized (DI) water to dissolve remaining salts and free the Cu-MXene product. This is washed 3 times with DI water to remove residual salts. To dissolve the copper deposited on the MXene surfaces, the washed Cu-MXene is first added to a solution of 2M HCl/1M $CuCl_2$, using 4x the mass of $CuCl_2$ used for the original synthesis. This is stirred, typically for 4h (times as short as 30m can be used but some Cu may remain) and then washed with DI water until a neutral pH (~5-6) is achieved. Finally, the wet powders of MXene are dried using vacuum filtration. After the bulk water is removed, 3 portions of 50mL of absolute ethanol are used to speed drying. The dry powders are vacuum annealed at 200 ˚C for 4h to remove intercalated water.

We have also been able to delaminate $Ti_3C_2Cl_2$. Because the halogen terminations lead to a hydrophobic MXene, the annealed product is first transferred into an argon filled glove box. To intercalate, 1.2g of LiCl (anhydrous, Sigma) is added to 10 mL of dimethyl sulfoxide (DMSO, Sigma) with a PTFE stir bar and stirred to dissolve, about 10 minutes. Then 1g of the annealed MXene is added to this solution and stirred on a stir plate for 24 h at 1000 rpm. To swell the intercalated slurry, it is transferred into a 15mL centrifuge tube and centrifuged to remove extra intercalating solution. The product is then washed twice with THF (anhydrous, Sigma), with all supernatants discarded. Then the product is dispersed in 15ml of N-methyl formamide (NMF, anhydrous, Sigma) and washed several times until significant volume expansion is observed. This can be delaminated in either NMF or other solvents, such as acetonitrile. To delaminate in NMF, the suspension is sonicated in an ice bath for 30m. The sonicated mixture is then centrifuged at 3500 RPM, yielding single and few layer flakes in the supernatant. To use ACN instead of NMF, excess NMF is discarded, and replaced with acetonitrile (ACN, Sigma), followed by the sonication steps above. Delamination of other molten salt MXenes is an ongoing challenge.

2.2 Chemical functionalization and hybridization of EMs

The details on the hybrid and functionalized electrode materials and their characterizations, are provided in deliverable D2.2.

2.3 Procedures for the formulation of aprotic ILs for EDLCs

These compounds were mostly produced in a two-step process consisting of the quaternisation of the amine (producing the desired cation) followed by metathesis (producing the desired anion). Exact details concerning the production and purification of ILs is confidential and based on Solvionic's trade secrets know-how. These ILs were purified as to obtain products with the necessary quality required for electrolytes (purity >99.9%, water content < 5 ppm, halide content <1 ppm et amines <10 ppm). Smaller quantities of ionic liquids were produced batchwise whereas larger quantities were produced on a continuous flow reactor line. The chemical pathways developed for the synthesis and purification of these ILs were conceived specifically with industrialisation in mind (easy upscaling, safety, toxicity and REACH).

All ionic liquids were handled, stored and formulated inside a MBRAUN LABmaster pro glove box, which is filled with argon and maintains H_2O and O_2 levels below 1 ppm. All solvents used for electrolytes were priorly dried with molecular sieves and their water content was verified before formulation (<10 ppm). Samples were stored and shipped in airtight aluminium or plastic flasks under Ar ensuring minimal contamination or alteration of the electrolytes.

2.3.1 Procedures for the Synthesis of Protonated ILs for MXenes

Exact details concerning the production of ILs is confidential. The production, handling and formulation of protic ionic liquids is performed in the same conditions as the aprotic ILs. Water content in these samples was slightly higher than for aprotic samples given the more hydrophilic nature of these compounds.

2.4 Physicochemical Characterization of electrolyte

Ionic conductivity was measured using a BioLogic MPG-2 potentiostat in a Binder KB53 climatic chamber, over a temperature range of -30 °C to 80 °C. Viscosity was assessed using a Rheometer MCR 102 (PerkinElmer) from -20 °C to 30 °C at a shear rate of 1000 s^{-1}. Density measurements were performed with a DMA 4000 (Anton Paar) between 0 °C and 80 °C. Thermal stability was evaluated by thermogravimetric analysis (TGA) on a PerkinElmer STA 6000 from 30 °C to 500 °C, using a heating rate of 10 °C/min.

2.5 Electrochemical characterization of electrode/electrolyte interfaces

To evaluate the electrochemical performance and stability of electric double-layer capacitors (EDLCs) at room temperature, a range of electroanalytical techniques were employed. These included cyclic voltammetry (CV), galvanostatic cycling with potential limitation (GCPL), and electrochemical impedance spectroscopy (EIS). EIS measurements were carried out over a broad frequency range from 100 kHz to 100 mHz. To investigate the influence of the electrolyte on the long-term stability of the EDLC cells, float tests were conducted at upper cut-off voltage of a cell. To monitor performance degradation, charge-discharge cycles were carried out periodically in between every 10 hours throughout the float test. The effect of the respective electrolytes on the anodic dissolution of aluminum (Al) current collectors has been also investigated using advanced CV. In this case, Al metal

discs (12 mm diameter) were used as the working electrode, an oversized activated carbon electrode (having active mass > 50 mg) as the counter electrode and an Ag-wire as a reference electrode. The Al electrode was polarized up to a potential of 1.5 V versus Ag wire using a scan rate of 0.5 mV s^{-1}. After reaching the upper potential limit, the electrode was held at that potential for 3 hours before the scan direction was reversed. This entire cycle was repeated 10 times to simulate extended anodic exposure. To quantify the extent of anodic dissolution, the cumulative anodic current was determined by integrating the recorded current over time.

The electrochemical performance of EDLCs was also evaluated at elevated temperatures using operando temperature-dynamic (TDyn) measurements conducted between 20 °C and 80 °C. Galvanostatic CD profiles and EI spectra were recorded at 5 °C intervals over a frequency range of 100 kHz to 100 mHz.

Finally, the specific capacitance *C* [F g^{-1}] for the cell has been calculated by following equation:

$$C = \frac{I}{(\Delta V/\Delta t) * m}$$

Where, *I* (A) represent the constant applied current, *m*(g) is the total active mass of both electrodes and $\frac{\Delta V}{\Delta t}$(V s^{-1}) the slope of the discharge curve.

3 Results & Discussion

3.1 Synthesis of CRM-Free MXenes

3.1.1 Synthesis of CRM-Free MXenes by mild etching

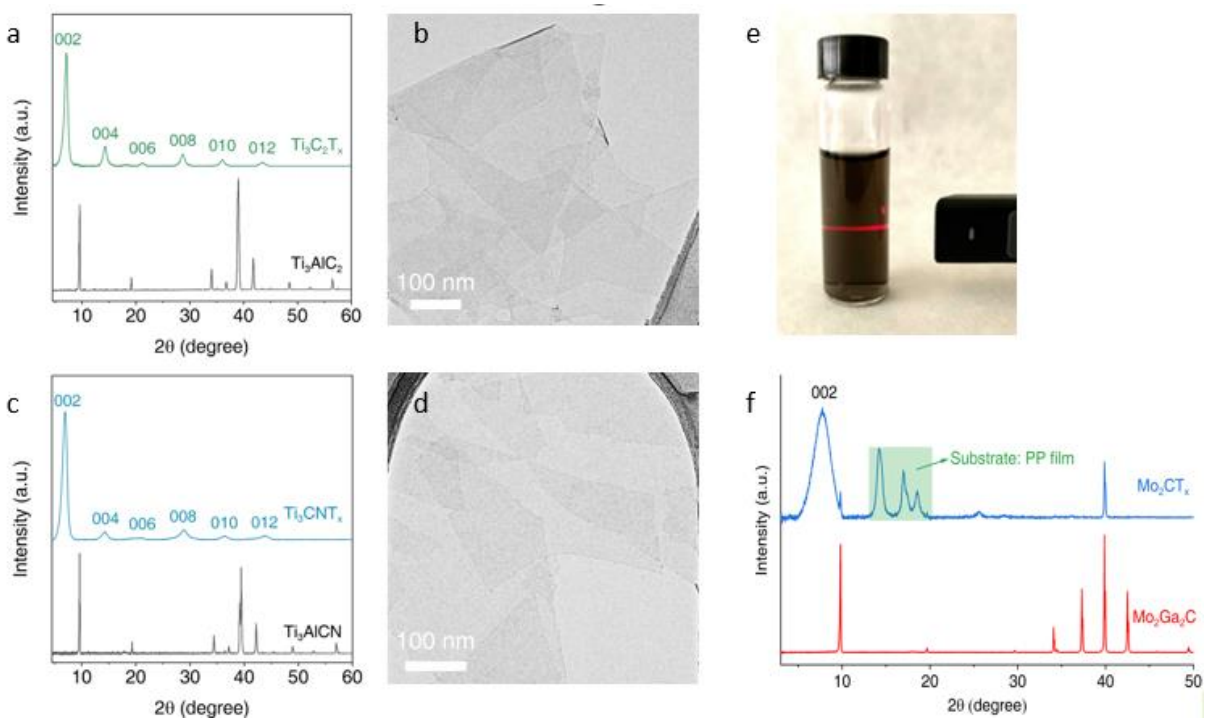

Figure 1. *A summary of MILD etching of MXenes. XRD patters of MILD etched $Ti_3C_2T_x$ (a), Ti_3CNT_x (c), and Mo_2CT_x (f) in comparison to their parent MAX phases, TEM of single and few layer flakes of $Ti_3C_2T_x$ (b) and Ti_3CNT_x (d). (e) A dilute colloidal solution of $Ti_3C_2T_x$ flakes demonstrating the Tyndall effect is shown in (e).*

MILD etching of MXenes has been used to produce $Ti_3C_2T_x$, Ti_3CNT_x, and Mo_2CT_x (from Mo_2Ga_2C). The etching of both titanium-based MXenes has been well reported in the literature, and we are able to produce robust quantities of both of these MXenes. Delamination of $Ti_3C_2T_x$ has been successfully scaled to produce multiple grams of MXene by using a high-capacity vortex mixer/shaker. Furthermore, freezing the wet MXene allows intercalated water to form ice crystals, which expand the interlayer spacing and facilitate delamination. It is possible to produce multiple grams of delaminated MXene per week with this method.

Mo_2CT_x has also been etched using the MILD method. This is most commonly produced with hydrofluoric acid, but the MILD method is an available method as well. The yield for Mo_2CT_x is not as good as with the Ti-based MAX phases (of which up to 80% of the weight can be converted into delaminated flakes), but delaminated MXene can be produced with this method. Increasing etching time or temperature may be able to produce more robust delamination.

3.1.2 Synthesis of CRM-Free MXenes by molten salt etching

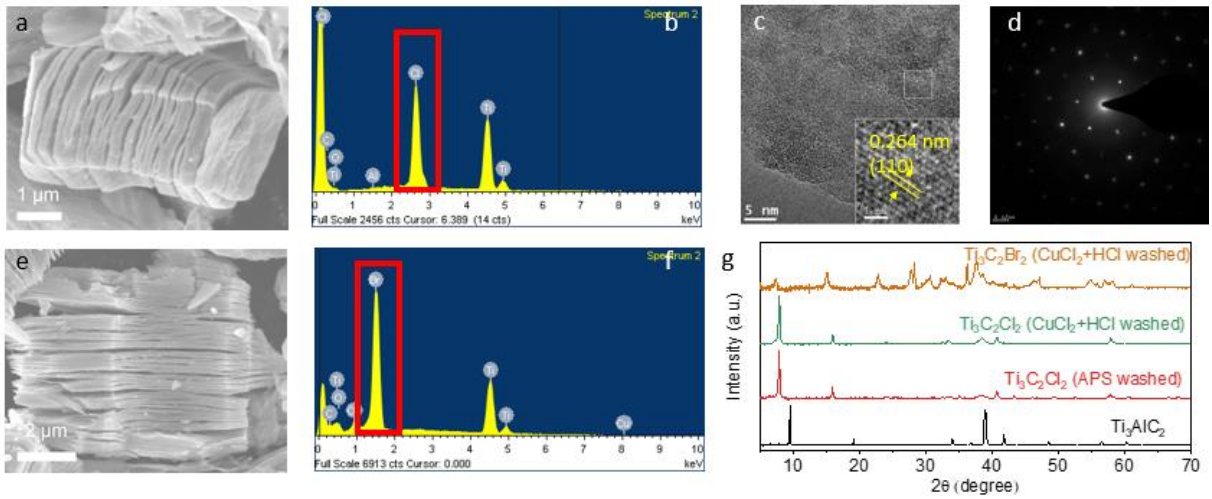

Figure 2. *Results of molten salt etching of $Ti_3C_2T_x$ with two salt compositions. SEM (a) and EDS spectrum (b) of $Ti_3C_2Cl_2$. TEM (c) and SAED (d) of $Ti_3C_2Cl_2$. SEM (e) and EDS spectrum (f) of $Ti_3C_2Br_2$. XRD patterns (g) of $Ti_3C_2Br_2$ washed with $CuCl_2$ and HCl, $Ti_3C_2Cl_2$ washed with either $CuCl_2$ or APS, and Ti_3AlC_2.*

Molten salt etching has been used to produce a wide swathe of MXenes from their parent MAX phases. Ti_2AlC, Ti_3AlC_2 (both stoichiometric and Al-rich), Ti_3AlCN, Mo_2Ga_2C, Mo_2GaC, $(Mo_{2/3}Y_{1/3})_2AlC$, $Mo_2Ti_2AlC_3$ have all been converted into their MXenes. For most of the above, the same synthesis can be used. Ti_2AlC, Ti_3AlC_2 (both stoichiometric), Ti_3AlCN, Mo_2GaC, and $Mo_2Ti_2C_3$ use a ratio of 1:3:3:3 of the MAX phase with KCl, NaCl, and $CuCl_2$ and are then processed for 5 hours at 700 ˚C. Mo_2Ga_2C requires more of the salts (1:6:6:6 ratio), due to the extra gallium in the structure, but the processing conditions remain the same. $(Mo_{2/3}Y_{1/3})_2AlC$ requires more time (12 h at 700 ˚C), but the 1:3:3:3 ratio of salts is sufficient.

Ti_3AlC_2 can be made with either stoichiometric ratios of the elements, or with extra aluminum (Al-rich). Interestingly, the Al-rich MAX phase requires extra time to process with the molten salt etching. The 1:3:3:3 ratio and 5 h 700 ˚C etching conditions do produce MXene, but there is a significant amount of unreacted MAX left over. This could be explained by the difference in defect quantity for the Al-rich MAX phase. The use of extra aluminum reduces lattice defects in the MAX phase, but these defects may provide sites for the initiation of the etching process. We are still working on the optimal etching condition of the Al-rich MAX phase.

3.1.3 IL electrolytes for EDLCs

3.1.3.1 3Electrochemical studies of CG electrodes

Different types of aprotic ILs and/ or electrolyte salts including $Pyr_{13}FSI$, $N_{1113}FSI$, $Pyr_{14}BOB$, and $Pyr_{14}DFOB$ from SOLV were sent to FSU. The electrolytes were formulated with varying concentrations (1M and 2M) in ACN and used to evaluate the performance of CG-based EMs. The results of this study have been published.[1]

Initially, the ionic conductivities of the prepared electrolytes were measured using a Binder KB53 climatic chamber and a BioLogic MPG-2 potentiostat. The ionic conductivity was measured from -30 to 80 °C (**Figure 3a**). As expected, conductivity increased with rising temperature. Among the tested electrolytes the ammonium-based salts in ACN shows the highest conductivity across the entire temperature, regardless of the salt concentration and even better than that of state-of-the-art $TEABF_4$ electrolyte. On the other hand, $Pyr_{13}FSI$ salts exhibited lowest conductivity for both the selected concentrations. The difference in conductivity between N_{1113} and Pyr_{13} could be explained by the smaller size of N_{1113} cation compared to Pyr_{13}. Nonetheless, the conductivity values achieved with the investigated electrolytes are comparable to conventional electrolyte $TEABF_4$. Further, the viscosity of the electrolytes was measured from -20 to 30 °C (**Figure 3b**). The viscosity of the investigated electrolytes shows different trend than the conductivity and it decreases with increasing the temperature, as expected. The densities of electrolytes containing 2M of IL are higher than that of the state-of-the-art electrolytes over the entire investigated temperature range (Figure 3c). At 20 ^{0}C, the density of 1M $TEABF_4$ in ACN, 1M N_{1113} FSI in ACN and 1M $Pyr_{13}FSI$ in ACN are equal to 0.87 g cm^{-3}, 0.92 g cm^{-3} and 0.93 g cm^{-3}, respectively. **Table 2** shows a comparison of the conductivity, viscosity and density of the investigated electrolytes at 20 °C.

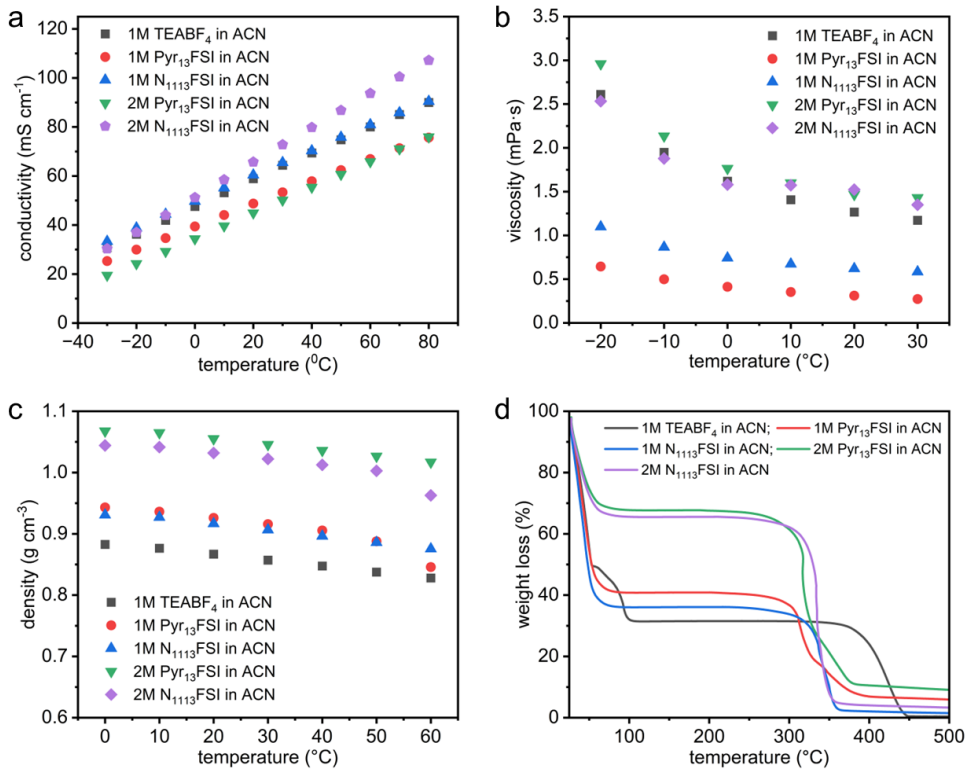

***Figure 3**. Physicochemical properties of investigated IL-based electrolytes over different temperature range: (a) conductivity; (b) viscosity; (c) density; and (d) thermal stability.*

***Table 2.** The relevant parameters measured for the investigated electrolytes at 20 ^{0}C.*

Electrolyte	Conductivity (mS cm^{-1})	Viscosity (mPa s)	Density (g cm^{-3})
1M $TEABF_4$ in ACN	58.8	1.27	0.87
1M $Pyr_{13}FSI$ in ACN	48.7	0.31	0.93
1M $N_{1113}FSI$ in ACN	60.4	0.62	0.92
2M $Pyr_{13}FSI$ in ACN	44.9	1.47	1.05
2M $N_{1113}FSI$ in ACN	65.6	1.52	1.03

Moreover, thermal stability of these electrolytes was investigated by thermogravimetric analysis (TGA) measurements between the temperature range of 30-500 ^{0}C (**Figure 3d**). The initial rapid mass loss observed between 30-50 ^{0}C for all electrolytes was due to the evaporation of volatile ACN solvent. Then, for all investigated electrolytes no significant weight loss is detected till 250 °C, indicating that the conducting salts is stable up to this temperature. Briefly, the investigated electrolytes display a comparable thermal stability with the 1M $TEABF_4$ in ACN. In summary, all investigated electrolytes show promising physicochemical properties and appears suitable for use as electrolytes in EDLCs.

After evaluating the chemical-physical properties of electrolytes, their use as electrolyte in EDLCs has been investigated with CG electrodes provided by SKL. As shown **Figure 4a**, the voltametric profiles display the typical rectangular shape in all tested electrolytes, indicating that no faradaic reactions are taking place in the considered voltage range. The charge-discharge profiles display triangular shape, high reversibility and small resistance in all electrolytes (**Figure 4b**). Importantly, during these tests the EDLCs display nearly similar capacitance values, regardless of the applied rates (**Figure 4c**) and those are higher than that of conventional $TEABF_4$ electrolyte. A comprehensive comparison of the specific energy and power of symmetrical EDLCs for all these cells is presented in a Ragone plot (**Figure 4d**). It is noted that the device with 2M $N_{1113}FSI$ electrolyte achieve an energy density of 34 Wh kg^{-1} and retains 82% of its performance even increasing the current density by ten-fold, demonstrating high-power capability (14 kW kg^{-1}). This observation highlights the potential of these electrolytes as suitable alternatives for commercial supercapacitors.

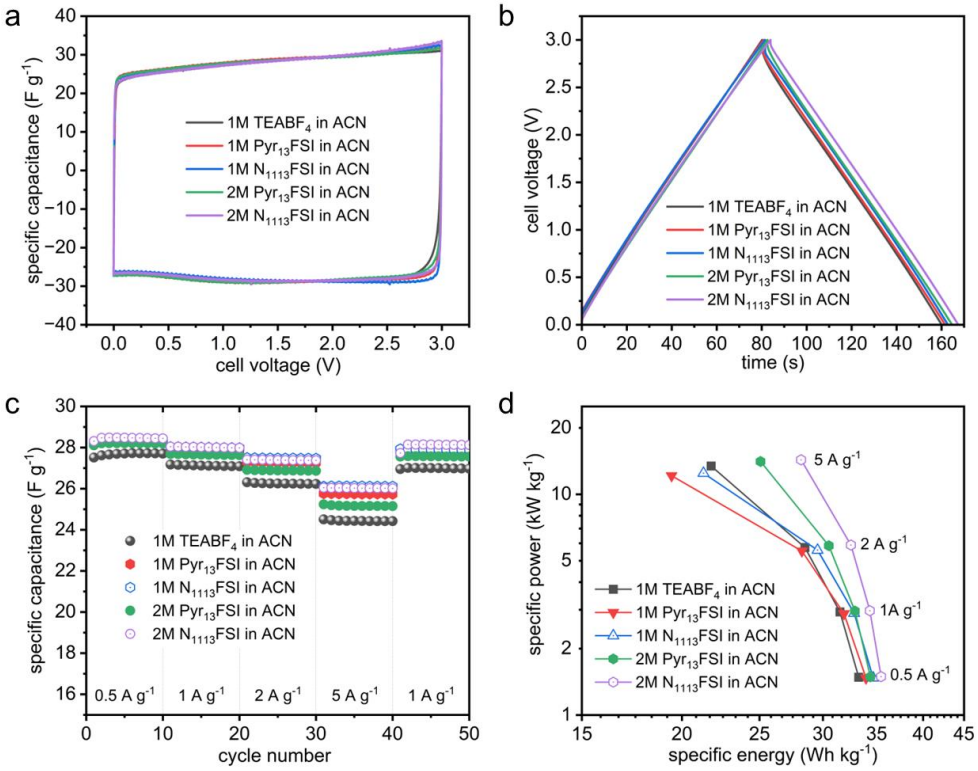

***Figure 4**. (a) comparative CVs at 5 mV/s; (b) charge-discharge profiles at 1 A/g; (c) rate capability; and (d) Ragone plot.*

We also evaluate the performance of EDLCs containing these alternatives electrolytes at elevated temperatures. Thus, operando temperature dynamic (TDyn) measurements were carried out in the temperature range comprise between 20 and 80 °C. The cells containing $Pyr_{13}FSI$ and $N_{1113}FSI$ electrolytes demonstrates a substantially stable response across the tested temperature range (**Figure 5**). In contrast, a gradual decrease in capacitance is observed for cell using the conventional $TEABF_4$ electrolyte as the temperature increases. This can be attributed to the limited thermal stability of the ACN solvent at elevated temperatures, leading to an increase in the total cell resistance. Afterwards, the effect of the temperature on the specific energy and power of the cells (at 3 V) was analysed. A decrease in energy density with increasing cell temperature is observed in all devices, regardless to the use electrolyte ($Pyr_{13}FSI$ and $N_{1113}FSI$). An increase of temperature leads to an increase of power since the ion mobility is increasing (which is in good agreement with observed physicochemical properties in **Figure 3**). However, the cell containing 2M $Pyr_{13}FSI$ in ACN shows a different behaviour, this behaviour is due to some change in the formation of the EDLC.

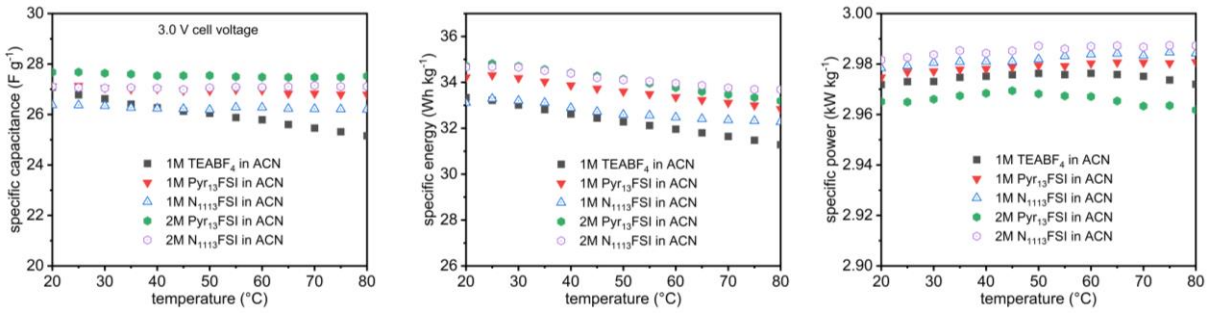

Figure 5. *TDyn evaluation for specific capacitance, energy density and power density for cell voltage of 3.0 V and current density of 1 A g^{-1}.*

To gain deeper insight into this observation, the EIS spectrum for the respective cell was analysed (**Figure 6**). All cells, except that containing 2M $Pyr_{13}FSI$, exhibit a decrease in charge-transfer resistance as the temperature increases. It is important to note that with rising temperature, the resistance Re(Z) shifts to lower values, while the height of the capacitive tail decreases. Additionally, higher temperatures result in reduced Warburg impedance, indicating improved transport properties, as expected.

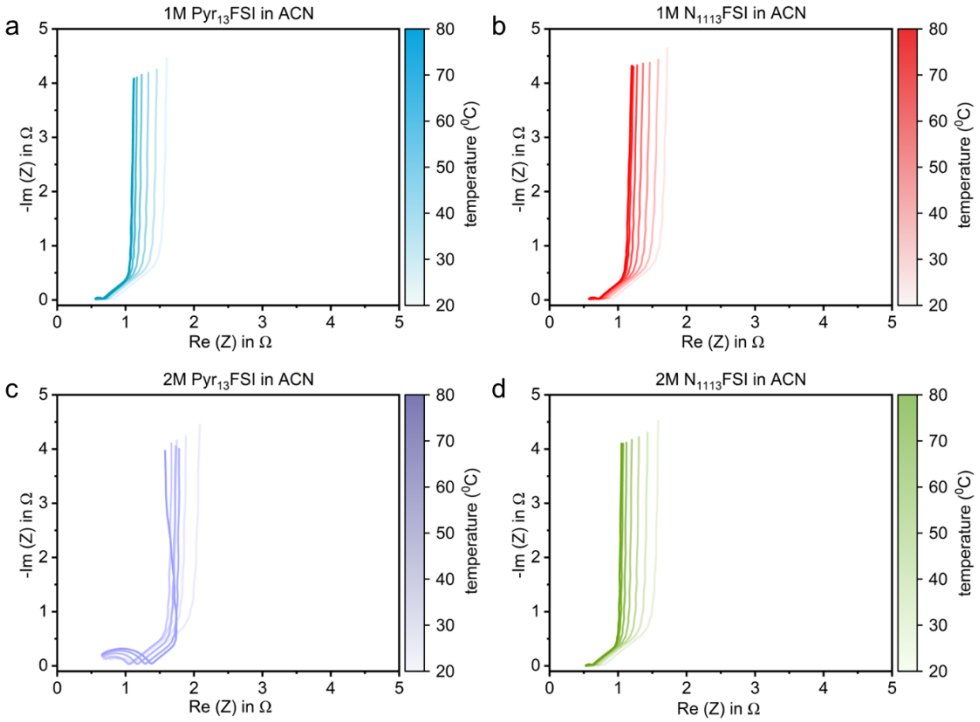

Figure 6. *Influence of temperature on EIS of symmetric EDLCs for (a) 1M $Pyr_{13}FSI$ in ACN; (b) 1M $N_{1113}FSI$ in ACN; (c) 2M $Pyr_{13}FSI$ in ACN; and (d) 2M $N_{1113}FSI$ in ACN.*

Finally, we assess the long-term durability of the cells by galvanostatic charge-discharge cycles and float test. All the tested cells exhibit good stability during charge-discharge cycles (**Figure 7a**). The cell containing 1M $TEABF_4$ in ACN displays good stability also during float test as well (**Figure 7b**). However, the stability of the cells containing $Pyr_{13}FSI$ and $N_{1113}FSI$ was lower. The cells containing 2M of these ILs

display better retention than those containing 1M, however they were still less stable than the cell containing the conventional electrolyte. The differences in stability are possibly associated to the different abilities of these electrolytes to suppress the anodic dissolution of the Al current collectors. To validate this assumption, we conducted a detailed examination of the anodic dissolution of Al current collectors (**Figure 7c**). In the electrolytes containing the $Pyr_{13}FSI$ and $N_{1113}FSI$ the Al current collectors start to dissolve within few hours, as indicated by the strong increase in the cumulative current. Also, increasing the salt concentration (from 1M to 2M) reduces the reaction kinetics (**Figure 7d**). However, this increase of concentration does not completely suppress the occurrence of anodic dissolution as in the case of the conventional electrolytes. We also incorporated secondary additives ($Pyr_{14}BOB$ and $Pyr_{14}DFOB$) to the electrolyte to mitigate the anodic dissolution. Nonetheless, float stability remains insufficient (results are not shown here). Our findings highlight the critical influence of electrolyte composition on anodic dissolution of Al current collector and overall stability of EDLCs.

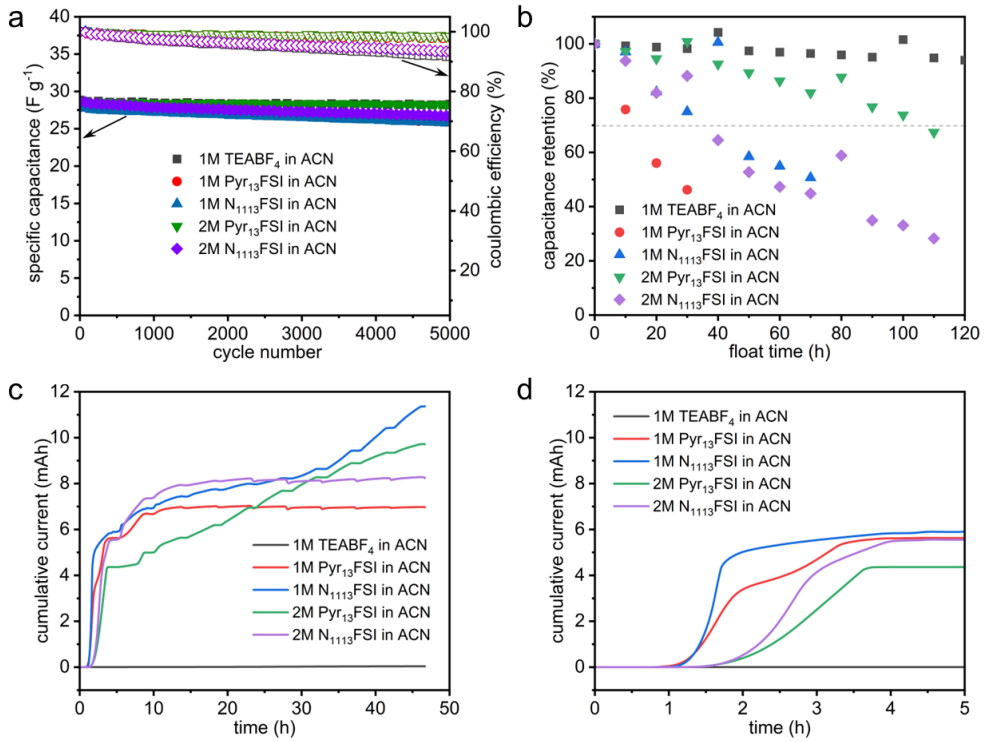

***Figure 7**. (a) cycling stability carried out at 1 A g^{-1}; (b) float test stability conducted at 3V; (c) anodic dissolution of Al current collector; and (d) zoomed-in view of the initial few hours of anodic dissolution.*

In conclusion, the use of the alternative aprotic electrolyte based on $Pyr_{13}FSI$ and $N_{1113}FSI$ appears promising. However, the stability of EDLC containing these electrolytes during float test at 3V needs to be improved. Notably, insights from float analysis suggest that the FSI anion is not as effective as the BF_4 anion in preventing the anodic dissolution of Al current collectors.

3.1.3.2 IL electrolytes with solvents

Based on its properties, as well as encouraging electrochemical performances measured by various partners in SCs based on CG- and AC/FLG-based electrodes, 1M $N_{1113}FSI$ in ACN was selected from the range of candidates developed in WP1. This is considered the 1st generation of Greencap electrolytes.

Unfortunately, as observed by Skeleton in initial trials in cylindrical cells (WP4), the $N_{1113}FSI$ in ACN electrolyte underwent degradation when held at 3.0V (floating test) at 65°C. These harsher conditions allow for testing the ageing in an accelerated manner. The degradation of those systems with $N_{1113}FSI$ in ACN was associated with corrosion of Al. Indeed, compared to BF_4 which effectively passivates aluminium, FSI forms no passivation layer which allows for aluminium corrosion and dissolution on the positive side at high potentials. Following these results, a range of other IL based electrolytes were explored at SOLV, using BF_4 and TFSI anions, using the SKL protocol. The ionic liquids selected were 1-Ethyl-3-methylimidazolium tetrafluoroborate ($EMImBF_4$), 1-Ethyl-3-methylimidazolium bis(trifluoromethylsulfonyl)imide (EMImTFSI), N-Methyl-N-propylpiperidinium bis(trifluoromethylsulfonyl)imide ($PI_{13}TFSI$), N-Methyl-N-propylpyrrolidinium bis(trifluoromethylsulfonyl)imide ($Pyr_{13}TFSI$), N-Methyl-N-methylpyrrolidinium tetrafluoroborate ($Pyr_{11}BF4$) and N-Methyl-N-propylpyrrolidinium tetrafluoroborate ($Pyr_{13}BF4$), see Error! Reference source not found.. These were formulated as 1.0 M or 1.2 M in acetonitrile. These ILs move away from FSI anions whilst also having a variety of cations with different stability and conductivity properties.

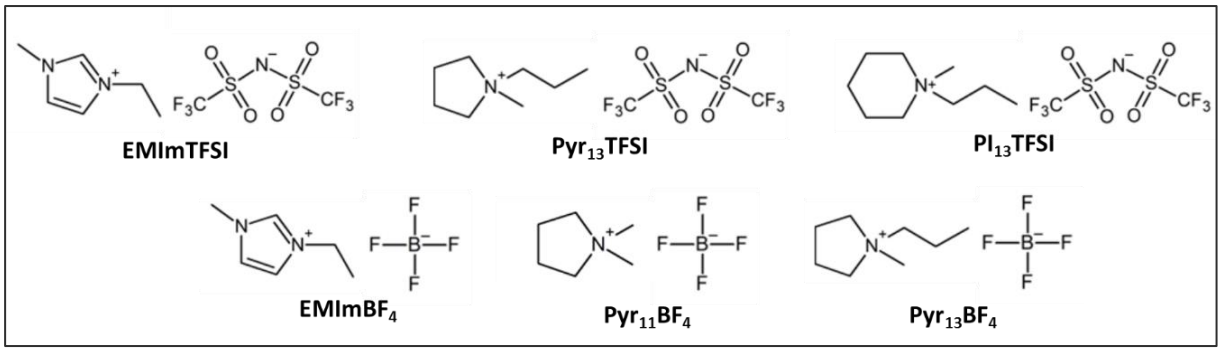

Figure 8. *Structure of Greencap's "2nd generation" electrolytes.*

In the first stage, as to measure the cell specific capacitance with the different electrolytes they were cycled in a three electrode Swagelok cell, see Error! Reference source not found.. All the electrolytes demonstrate typical EDLC behaviour (i.e. linear increase/decrease in potential at a fixed current). The highest cell specific capacitance was measured with $EMImBF_4$ (25.6 F/g) and the lowest was measured with $PI_{13}TFSI$ (21.2 F/g). Importantly, no electrolyte appears to undergo marked degradation or redox reactions.

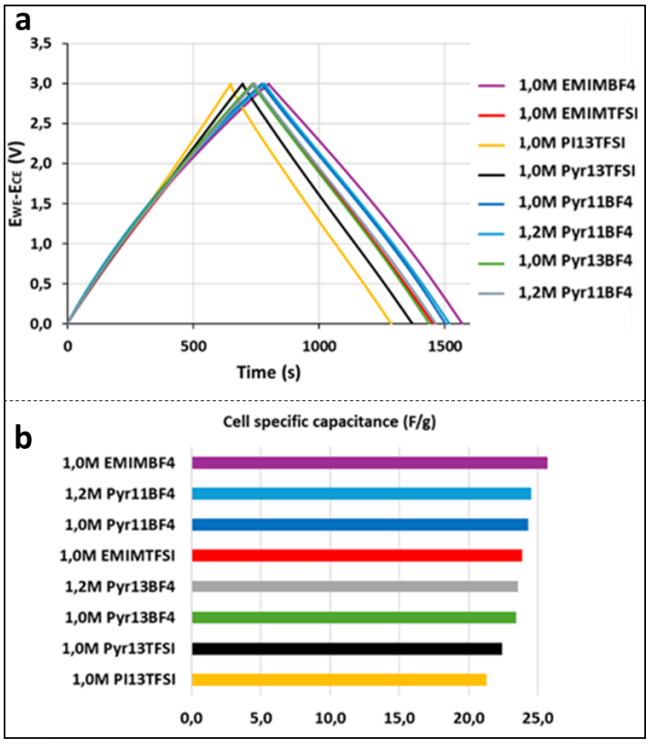

Figure 9. *(a) Galvanostatic charge/discharge (0.1 A/g; 0 to 3.0V) profiles of "2nd generation" electrolytes with CG Gen 2 electrodes (8-9 mg/cm²); (b) Cell specific capacitance of the different electrolytes.*

Next, cells were floated at 3.0V at 65°C. As recommended by SKL, a positive to negative active mass ratio of approximately 1.2 was employed. For all the electrolytes, except for $Pyr_{11}BF_4$ and $Pyr_{13}BF_4$, the cells underwent rapid degradation and did not survive the first 120 hours of floating. In those cells, electrolyte discoloration occurred (symbolic of electrolyte degradation) and/or the aluminium current collector on the positive electrode underwent corrosion/dissolution as showed in Error! Reference source not found. for EMImTFSI. For that electrolyte, the capacitance decreased from 24.0 F/g to 0.8 F/g accompanied by an increase in ESR from 8.02 Ω/cm² to 67,1 Ω/cm² after 120h of floating at 3.0V at 65°C.

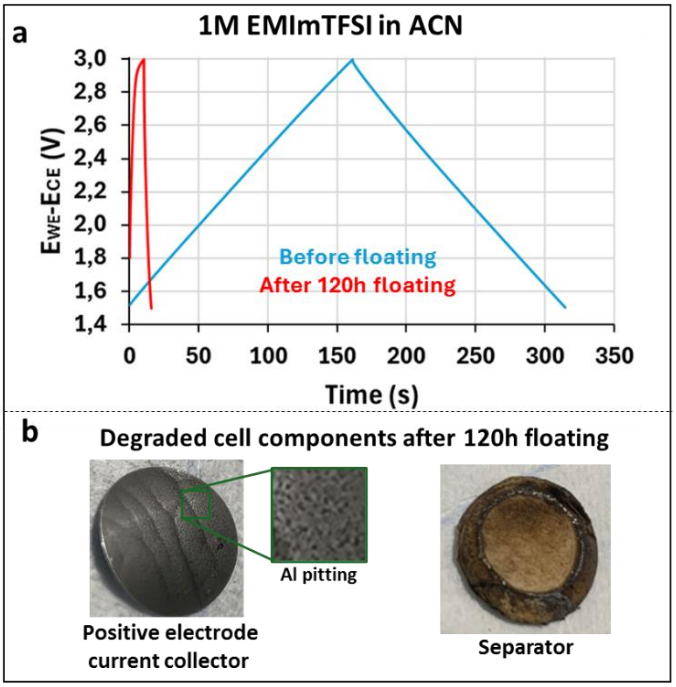

Figure 10. *(a) Galvanostatic charge/discharge profiles of 1M EMImTFSI in ACN measured at room temperature before and after 120h of floating at 65°C at 3.0V (10mA/F); (b) Photographs of cell components after 120h floating.*

For $Pyr_{11}BF_4$ and $Pyr_{13}BF_4$, the cells displayed better stability, mostly achieving 240h before undergoing degradation as shown in Error! Reference source not found.. The only exception was for the 1M $Pyr_{11}BF_4$ in ACN which began to degrade after 120h. The initial capacitance for all these electrolytes is similar, around 25 F/g.

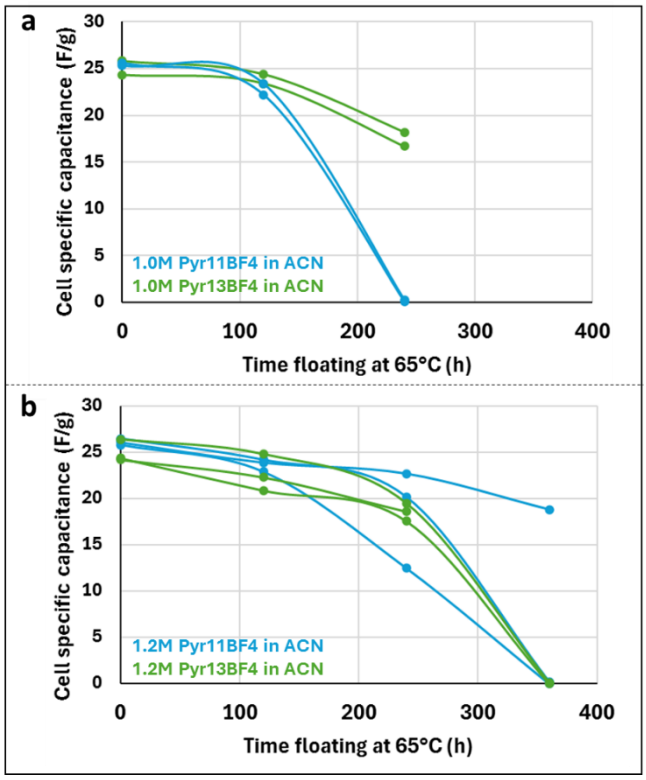

Figure 11. *Variation of cell specific capacitance during floating at 65°C for 1M (a) and 1.2M (b) electrolytes based on* $Pyr_{11}BF_4$ *(blue) and* $Pyr_{13}BF_4$ *(green). Bottom: Photograph of cell components at different points of life.*

When the cells died, postmortem inspection revealed that the coin cell casing (Al clad stainless steel) degraded, possibly before the electrode or the electrolyte. Indeed, it was observed that the stainless steel underneath the Al cladding corroded, leading to Al delamination, see Error! Reference source not found.. This could be due to inefficient or heterogeneous deposition of the Al on the stainless-steel casing. In those cases, the electrolyte remained didn't turn brown and the Al current collector remained intact, indicating an absence of electrolyte degradation and Al corrosion. For this cell format and components, surviving 240h of floating is a good result and indicates that these electrolytes are potentially exploitable for the prototypes.

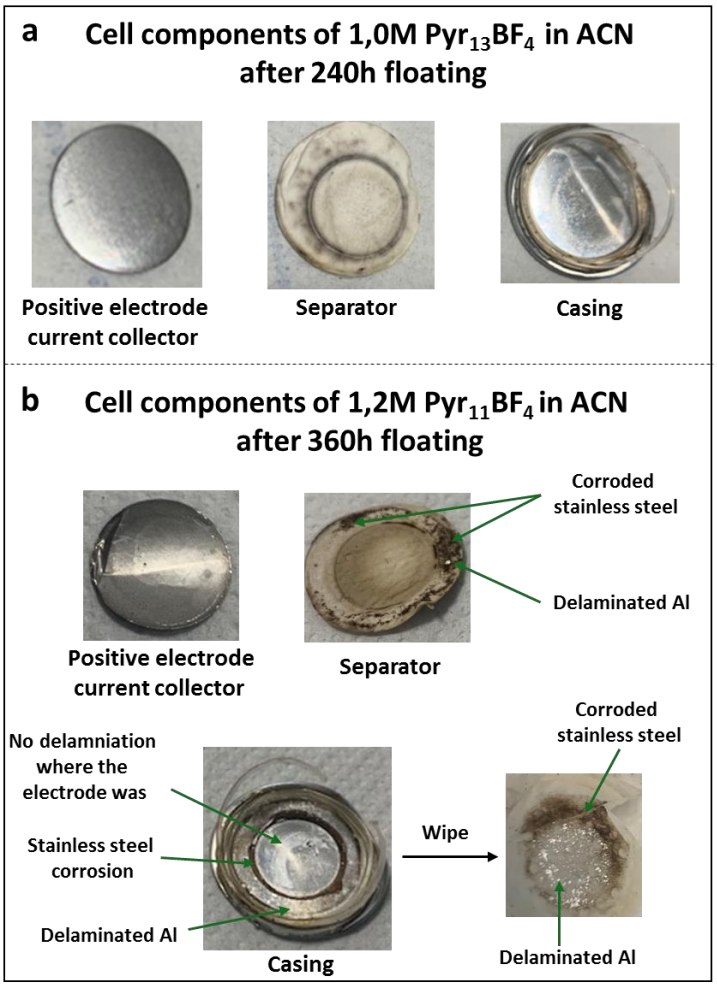

Figure 12. *Photograph of cell components at different points of life.*

Given these results, the $Pyr_{11}BF_4$ and $Pyr_{13}BF_4$ were chosen as the "2nd generation" of Greencap electrolytes for the project. Their upscaling is currently being developed at SOLV. Larger batches (kg scale) of 1M $Pyr_{11}BF_4$, 1.2M $Pyr_{11}BF_4$ and 1M $Pyr_{13}BF_4$ in ACN were send to SKL for WP4 and smaller batches were sent to other partners for further development.

3.1.3.3 IL filled electrodes

In this section, the work carried out on IL filled electrodes at SOLV will be described in relation to low temperature applications. BED and SOLV explored high temperature applications. and have published these results.[2] As described in D2.2, as to achieve -50°C operations, it is necessary to employ a "eutectic mixture" of ionic liquids which does not undergo any phase transition down to -50°C. The EMImFSI ILs used in ionogels for high temperatures cannot be used as it presents a melting point of approximately -14°C. One eutectic mixture developed earlier in the Greencap project was EMImFSI/BMImFSI (50/50 wt.%). Using this electrolyte, a cell was produced with a CG/PTFE (95/5 wt.%) electrode (9 mg/cm²) (see D2.2) and cycled at temperatures down to -50°C, see **Figure** . For this test, a potential of 2.6V was used to avoid any type of electrolyte degradation.

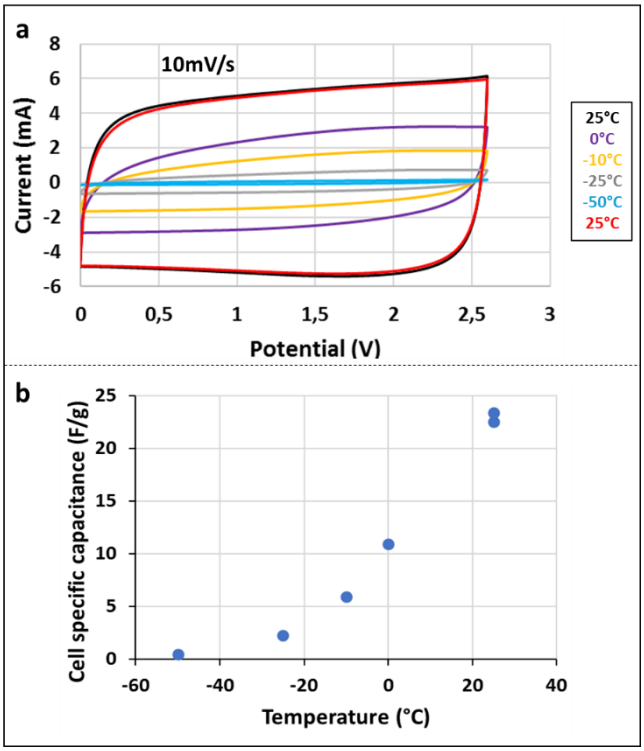

Figure 13. *Cyclic voltammetry profiles and cell specific capacitance of a coin cell composed of CG/PTFE electrodes (95/5%wt; 9.1 mg/cm²) and EMImFSI/BMImFSI (50/50%wt). Scan rate: 10mV/s; Potential: 0-2.6V; 5 CVs at each temperature.*

It was observed that the cell was capable of cycling at temperatures down to -50°C. As a point of comparison, in the same conditions with EMImFSI, the cell completely ceased to function at -25°C, supposedly due to electrolyte crystallization. For EMImFSI/BMImFSI, no important changes in the CV were observed when returning to 25°C after exploring the lower temperatures, suggesting that no irreversible reactions occurred. Nonetheless, a rapid drop in capacitance was observed when lowering the temperature. Approximately half the initial capacitance fading at 0°C and less than 1 F/g of cell specific capacitance remaining at -50°C. This can be associated with two possible factors: increased viscosity at low temperature and low ionic diffusion within the electrodes. Two approaches can be combined to address this issue; the first is to use a less viscous electrolyte and the second is to use IL filled electrodes.

As described in D2.2, an optimized eutectic mixture of ionic liquids was developed (EMImFSI/PMImFSI) with low viscosity and IL-filled curved graphene electrodes were produced. The objective here is to evaluate the electrochemical properties of these IL-filled electrodes with the IL electrolytes. They were produced using curved graphene (CG), polytetrafluoroethylene (PTFE) and different ILs based on Solvionic's patented know-how on ionogels.[3] An overview of the electrode properties is found in **Table** .

Table 3. *Composition of electrodes*

	AM loading (mg/cm²)	Thickness (mm)	%IL	%CG	%PTFE
Pyr13FSI/CG/PTFE	9.10	0.21	68.3	29.5	2.1
EMImFSI:PMImFSI/CG/PTFE	9.22	0.18	64.7	33.9	2.4

The electrochemical measurements were performed in a three-electrode configuration using a Swagelok type cell in Teflon (stainless steel pistons, platinum current collectors, glass fiber (Type A) separator) and the corresponding ionic liquid electrolyte ($Pyr_{13}FSI$ or 50/50 wt.% mixture of EMImFSI/PMImFSI). A silver wire was used as the reference electrode. Firstly, EIS was performed, see Error! Reference source not found.. This revealed a significant difference between the $Pyr_{13}FSI$ and EMImFSI/PMImFSI electrodes. The electrode resistance is significantly higher for $Pyr_{13}FSI$ (3,3 Ω/cm²) than for EMImFSI/PMImFSI (0.69 Ω/cm²). Similarly, at lower frequencies, a steeper slope is observed in the case of EMImFSI/PMImFSI compared to $Pyr_{13}FSI$ which indicate a better capacitive behaviour. All these observations indicate that cells with EMImFSI/PMImFSI electrode have more favourable properties compared to $Pyr_{13}FSI$ for EDLCs.

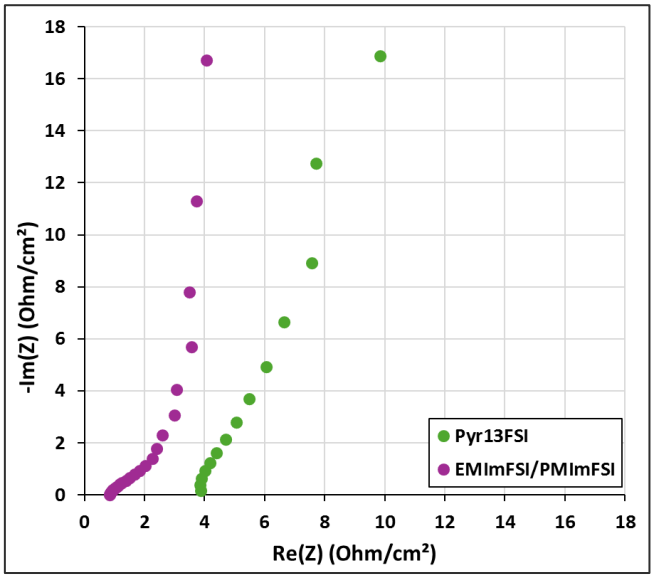

Figure 14. *EI spectra of three electrode Swagelok cells composed of $Pyr_{13}FSI$ (green) or EMImFSI/PMImFSI (purple) filled CG electrode (10 mHz to 1MHz with 10mV sinus amplitude).*

The cell with EMImFSI/PMImFSI was then cycled via CV at 10 mV/s at increasing potentials, see Error! Reference source not found.. The CV profiles up to 3.0V demonstrate typical EDLC behaviour with a square-like charge discharge profile and with coulombic efficiencies above 99%. At 3.2V however an irreversible increase in current density appears and the coulombic efficiency drops below 99% which are characteristic effects of parasitic faradaic reactions such as electrolyte degradation. As to avoid these reactions, it is preferable to cycle cells up to 2.8V or 3.0V.

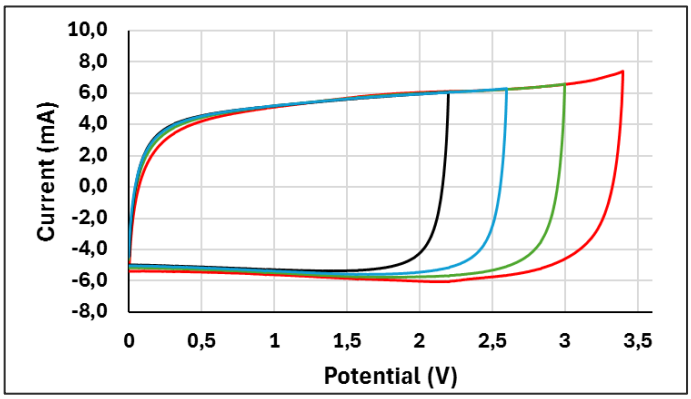

Figure 15. *CV of a cell composed of EMImFSI/PMImFSI CG electrodes at different potentials (10 mV/s).*

Next, these cells were cycled *via* galvanostatic charge discharge from 0 to 2.8V with a current density of 0.5 A/g. Whilst both cells are capable of charging and discharging, the profiles are quite different as it can be seen in **Error! Reference source not found.**. As expected, the cell with EMImFSI/PMImFSI charges and discharges with much less resistance compared to the cell with $Pyr_{13}FSI$. An equivalent series resistance (ESR) of 2.59 Ω/cm² was measured for EMImFSI/PMImFSI compared to 4.51 Ω/cm² for $Pyr_{13}FSI$. Additionally, the significant non-linearity of the $Pyr_{13}FSI$ cell suggests a reduced rate of the charge transfer at the material surface, largely due to a larger cation. The working potential on each electrode is similar for both cells. On the negative electrodes, working potentials (ΔE_{neg}) of 2.02 to 1.81V are measured whereas working potentials (ΔE_{pos}) of 0.78 to 0.99V are measured on the positive electrode. This suggests that, at a later stage of development, electrode mass balancing may be required as to equalize these electrodes working potentials thus limiting premature degradation.

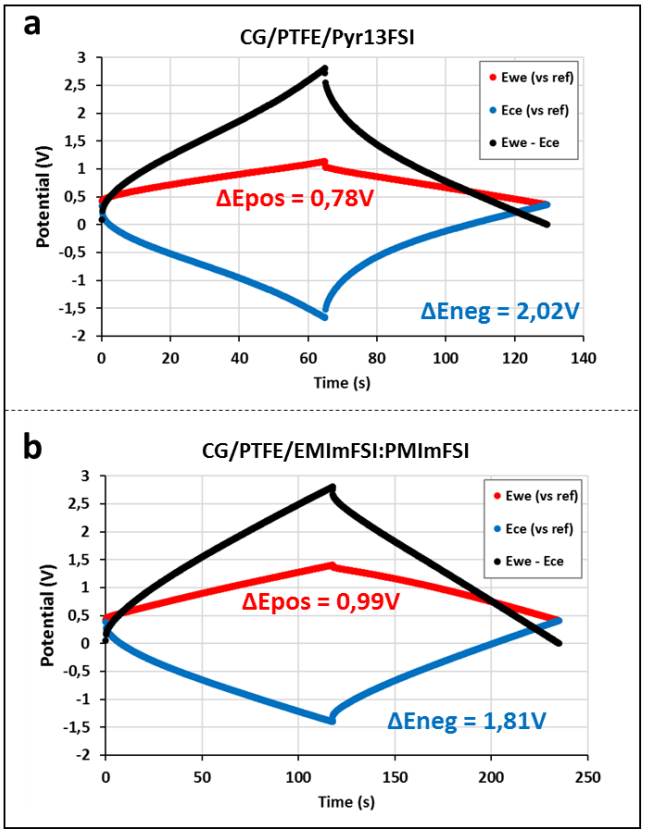

Figure 16. *Galvanostatic charge/discharge profiles of three-electrode Swagelok cells composed of $Pyr_{13}FSI$ (a) and EMImFSI/PMImFSI (b) filled CG electrode. Cycled from 0 to 2.8V at 0.5A/g (vs total active material weight).*

When compared to SKL electrodes of CG with similar loadings (8-9 mg/cm²), the IL-filled electrodes have better performance when using pure ionic liquids as electrolytes. Indeed, the EIS profile of cells composed of SKL's CG electrode are more resistive than the IL-prefilled equivalent (see **Figure 1**). Moreover, when charging and discharging, the GCD profile demonstrates a higher resistance and lower energy storage. These results could be associated with a much better mobility of ions within the IL-prefilled electrodes compared to classic electrodes.

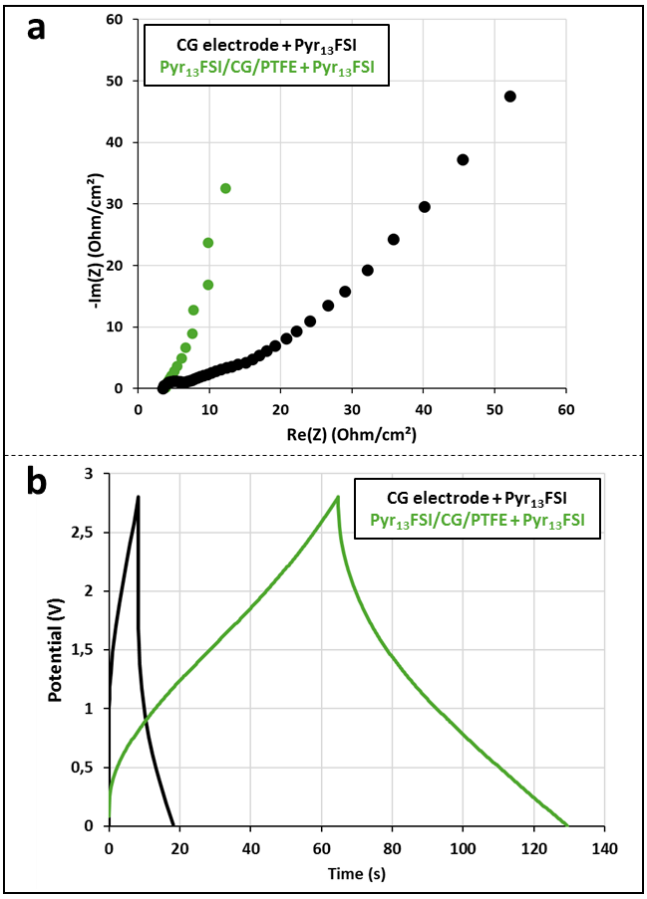

Figure 1. *EIS (a) and GCD (b) of coin cells composed of SKL's CG electrodes with $Pyr_{13}FSI$ electrolyte (black) and SOLV's $Pyr_{13}FSI$ filled CG electrodes with $Pyr_{13}FSI$ electrolyte (green). EIS: 10 mHz to 1MHz with 10mV sinus amplitude; GCD: Cycled from 0 to 2.8V at 0.5A/g (vs total active material weight).*

The IL-filled electrodes were then cycled over a long period in the same conditions (0-2.8V; 0.5 A/g), see

. EMImFSI/PMImFSI has a much higher cell specific capacitance (approximately 20 F/g) compared to $Pyr_{13}FSI$ (approximately 12 F/g). The $Pyr_{13}FSI$ based electrode cycled 10,000 times without much change in performance. These electrodes were sent to CNR for further analysis. However, for the EMImFSI/PMImFSI based electrode, there is a slight decrease in capacitance over time, which is accompanied by a decrease in coulombic efficiency, suggesting some type of degradation. This could potentially be associated to the imidazolium cations which are less electrochemically stable compared to pyrrolidinium cations. As mentioned above, improving the balance of the electrode could enhance this stability.

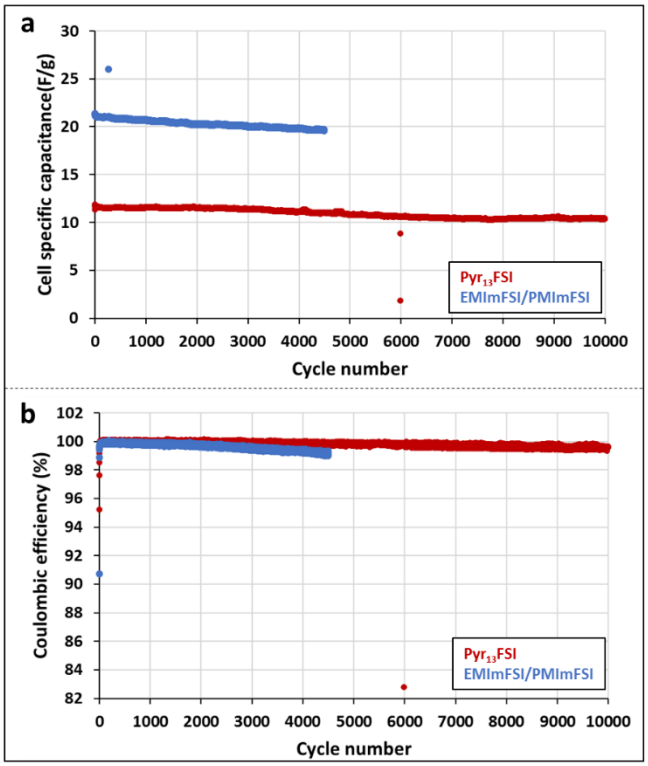

Figure 18. *Cell specific capacitance (a), cell specific energy (b) and coulombic efficiency (c) of cells composed of $Pyr_{13}FSI$ (left) and EMImFSI/PMImFSI (right) filled CG electrode. (0 to 2.8V with 0.5A/g (vs total active material weight).*

To conclude, the use of IL-prefilling improves the compatibility of pure ionic liquid electrolytes with active materials such as curved graphene. The integration of ILs during the production of these electrodes allows the production of electrodes with commercial loadings of active materials (9 mg/cm² and above) whilst greatly increasing conductivity and capacitance. In addition, the production of IL filled electrodes allows for the elimination of the drying step otherwise necessary when producing electrodes and eliminates the need for solvents such as NMP. The performance of these cells could be further fine-tuned by studying the effect of the proportions of the different electrode components, balancing the electrodes, varying the proportions of each electrode components and examining different binders and separators. Furter improvements in the scalability of this production method could come from the use of extrusion processes for electrode production and processing. In the next steps, these cells will be tested at temperatures of -50°C.

3.1.3.4 *Formulation of protic ILs for MXene*

A range of protonated ionic liquids (ILs) (N_{111H}TFO, Pyr_{1H}TFO and N_{111H}TFSI) were produced by **SOLV** for MXene EM (**Figure 19**). Protonated ILs were chosen in collaboration with FSU as to maximise electrolyte/MXene interaction via the H^+. Electrolytes were formulated with a range of various solvents: acetonitrile (ACN), propylene carbonate (PC) and water. ACN is the solvent used in the commercial supercapacitor (SC) electrolyte. Compared to ACN, PC is safer, less toxic and stable at higher temperature, thus permitting a broader range of applications within a wider temperature range. PC is nevertheless more viscous resulting in lower viscosity which ultimately limits devices power density. Water is obviously the ultimate green solvent although performance could be limited by water decomposition.

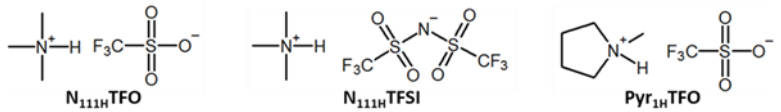

***Figure 19**. Details of the protic IL electrolytes produced and distributed to WP1,2 and 3 partners.*

The electrolyte density, conductivity and flash points were measured for those protic IL electrolytes. The results are reported in **Table 4**. These electrolytes achieve the target viscosity value (<20 mPa.s) but do not achieve the target electrochemical stability window (ESW) (4.5 V). The latter limitation could be due to the parasitic hydrogen evolution reaction caused by the presence of H^+. Compared to trifluoromethanesulfonate (TFO)-based ILs, bis(trifluoromethanesulfonyl)imide (TFSI)-based ones have larger ESWs. ACN and water electrolytes achieve the target conductivity value (>40 mS/cm for IL+solvents). PC-based electrolytes have much higher flashpoint than AC-based electrolytes. Higher concentration of electrolytes and IL binary mixtures will be explored to further improve the electrolyte properties.

***Table 4**. Conductivity, electrochemical stability window, conductivity, viscosity, density and flash point of 1mol/L protic IL electrolytes for MXenes.*

ILs	Solvent	ESW (V) (at 0.1 mA/cm² cut off)	Conductivity at 20°C (mS/cm)	Viscosity at 20°C (mPa.s)	Density at 20°C	Flash point (°C)
1M N_{111H}TFO	ACN	2,80	44,6	0,56	0,889	-
	PC	2,86	10,4	3,99	1,237	-
	H_2O	1,79	44,1	1,35	1,061	-
1M N_{111H}TFSI	ACN	3,31	67,1	0,66	0,963	-
	PC	3,28	12,1	4,40	1,285	-
1M Pyr_{1H}TFO	ACN	2,60	43,8	0,60	0,897	10
	PC	3,11	10,1	4,06	1,241	121
	H_2O	1,94	38,0	1,46	1,067	-
	ACN	3.00	53.8	0.93	0.979	-

2M N_{111H}TFO	H_2O	1.67	60.3	1.80	1.218	-

Electrochemical tests performed by partners showed that N_{111H}TFO is the most promising electrolyte of these three protic electrolytes. Given the higher concentration of classical MXene electrolytes (3M H_2SO_4, KOH…), electrolytes based on N_{111H}TFO with higher concentrations were formulated: 2M N_{111H}TFO in ACN and 2M N_{111H}TFO in water. These electrolytes present better conductivity although they are denser and more viscous compared to their 1M equivalents. In the case of 2M N_{111H}TFO in ACN, a slight increase of ESW was observed whereas the opposite was observed for 2M N_{111H}TFO in water.

In addition to these IL salts, a room temperature ionic liquid electrolyte for MXene, based on the 1-H-3-ethylimidazolium (EIH) cation and the TFSI anion was studied for MXene, see

Figure . This IL was developed because the initial tests of Ti3C2Tx with Pyr13FSI showed very little promise (high resistance and very low capacitance). It was suggested that a protic ionic liquid could improve the charge storage in the MXene systems. As these electrolytes contain no volatile solvents, they can be used at higher temperatures without risk of fire whilst also potentially being recoverable. The production of this ionic liquid was undertaken at SOLV and purification up to electrolyte grade (<20ppm water and >99.9% purity) was successful. This ionic liquid was used for 2 purposes: IL prefilling of Ti3C2Tx electrodes (see D2.2) and as an electrolyte for Ti3C2Tx electrodes

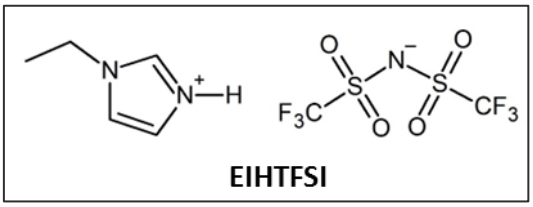

***Figure 20**. Structure of 1-H-3-ethylimidazolium bis(trifluoromethane)sulfonimide.*

Coin cells were made with EIHTFSI TCD's Ti3C2Tx electrodes (1.5 mg/cm²) then EIS and CVs at different potentials were performed. The EIS profiles of Pyr13FSI and EIHTFSI with Ti3C2Tx are very similar, Figure. The low slope of the curves at lower frequencies indicates that the charging process is restricted by ion diffusion processes in the electrolyte. Such highly resistive profiles are a sign of limited EDLC formation at the electrode leading to low energy storage.

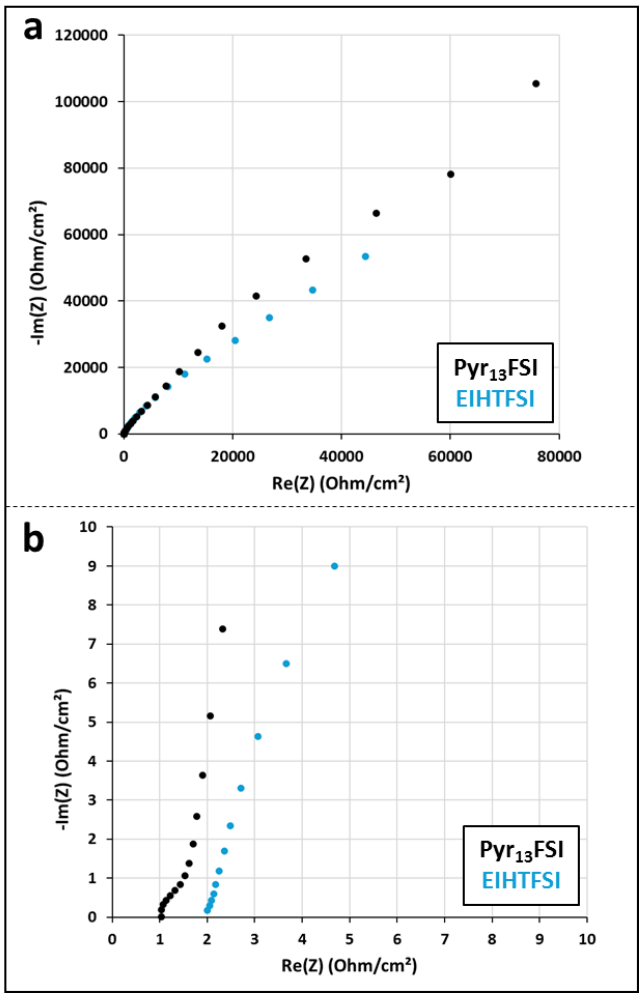

***Figure 21**. EIS of cell composed of $Ti_3C_2T_x$ and EIHTFSI (blue) and Pyr13FSI (black) electrolytes. a. 0 to 80 0000 ohm/cm²; b. 0 to 10 ohm/cm² (10 mHz to 1MHz with 10mV sinus amplitude).*

When examining the CV profiles for EIHTFSI, the current response is very low (<1 mA/g) and resistive, see **Figure 2**. At 1.0V the cell specific capacitance is <0.1 F/g which was also the case for $Pyr_{13}FSI$. When increasing the potential, a noticeable increase in current response appears at 1.6 V which is indicative of degradation.

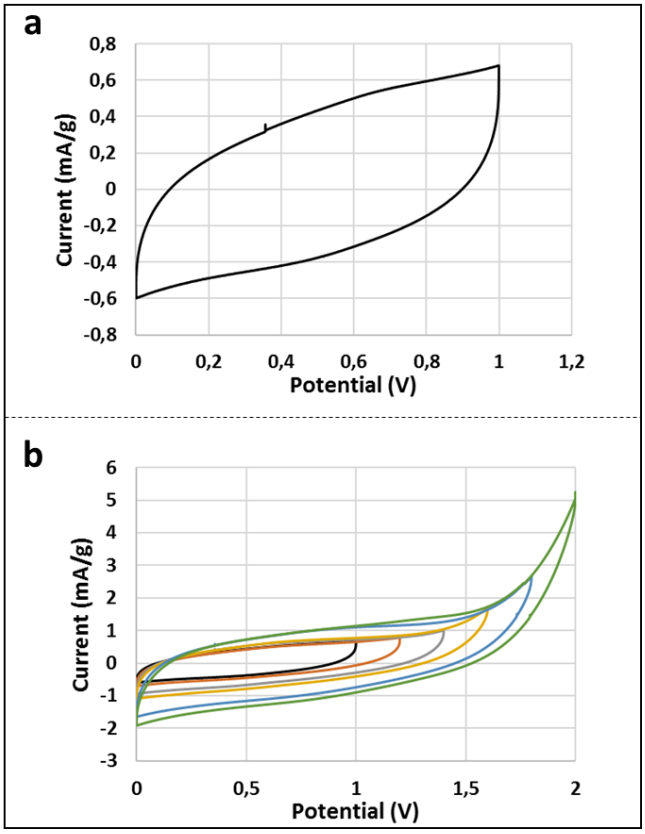

***Figure 2**. CVs of cells composed of EIHTFSI and $Ti_3C_2T_x$ electrodes (1.5 mg/cm²) between 0 and 1.0V (a) and at various potentials (b). 10 mV/s scan rate.*

In the conditions trialed, pure ionic liquids either protic (EIHTFSI) or aprotic ($Pyr_{13}FSI$) had limited compatibility with these $Ti_3C_2T_x$ electrodes. No improvement was observed for the protic EIHTFSI over the aprotic $Pyr_{13}FSI$. The performance of these systems could be improved *via* IL-prefilling of MXene materials (see D2.2) or by using an organic or inorganic acid dissolved within an ionic liquid. More encouraging results have been obtained with protic ionic liquids dissolved in acetonitrile and water. These trials will be renewed with an improved batch of $Ti_3C_2T_x$.

3.1.3.5 Electrochemical characterisation of $Ti_3C_2T_x$ MXene

FSU received 1M and 2M solutions of $N_{111H}TFO$ in both aqueous and organic solvents from SOLV. Initially, the temperature-dependent properties of protic ILs salt in water were systematically evaluated through conductivity, viscosity, and density measurements.

Figure 23a reveals the temperature-dependent conductivity behaviour of 1M and 2M $N_{111H}TFO$ in water. Both concentrations exhibit an increase in ionic conductivity with rising temperature, attributed to enhanced ion mobility. It's observed that the 2M solution shows higher conductivity than 1M counterpart, primarily due to the higher concentration of charge carriers. As shown in **Figure 23b**, viscosity decreases with increasing temperature. This trend is a result of reduced intermolecular interactions at elevated temperatures. **Figure 23c** displays the corresponding density profiles, which show a slight decrease with temperature, as expected. The 2M $N_{111H}TFO$ maintains a higher density

across the temperature range due to its higher solute content. A comparative summary of conductivity, viscosity, and density values for both electrolytes at 20 °C is provided in **Table 5**. The overall physicochemical properties of the investigated electrolyte are promising and indicate its suitability for further testing in MXene-based SC cells.

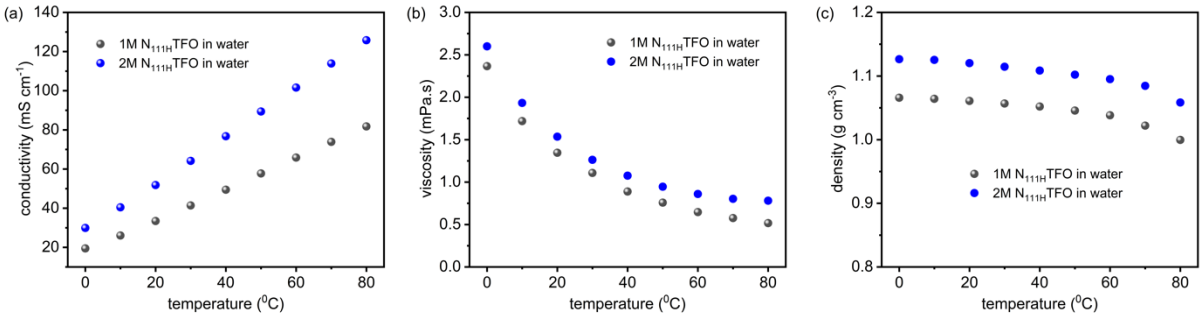

Figure 23. *Overview of (a) conductivity; (b) viscosity; and (c) density measured at various temperatures for protic IL electrolytes.*

Table 5. *Summary of conductivity, viscosity, and density for the investigated electrolytes at 20 ^{0}C.*

Electrolyte	Conductivity (mS cm^{-1})	Viscosity (mPa s)	Density (g cm^{-3})
1M N_{111H}TFO in water	33.45	1.35	1.0609
2M N_{111H}TFO in water	51.82	1.54	1.1202

FSU received the $Ti_3C_2T_x$ MXene sample from TCD, and the electrode fabrication was carried out at the FSU using aluminum (Al) current collectors, with a mass loading of nearly 0.5-0.7 mg/cm². The electrochemical performance of $Ti_3C_2T_x$ MXene electrodes was evaluated in protic IL electrolytes. These electrodes were initially tested in different concentration of N_{111H}TFO in water. To evaluate the performance of the $Ti_3C_2T_x$ MXene electrodes, measurements were conducted in a three-electrode Swagelok-type cell configuration. In this setup, the $Ti_3C_2T_x$ MXene served as the working electrode, a self-standing big fatty carbon electrode was used as the counter electrode, and an Ag wire functioned as the quasi-reference electrode. CV measurements were initially conducted to assess the electrochemical behavior of $Ti_3C_2T_x$ MXene electrodes in 1M/2M N_{111H}TFO aqueous electrolyte. As shown in **Figure 24(a-b)**, the CV curves exhibit nearly rectangular shapes, even at lower scan rates, which is characteristic of EDLC dominated charge storage. The absence of pronounced redox peaks suggests that charge storage occurs primarily through non-faradaic process, although slight deviations from ideal shape may be attributed to pseudocapacitive contributions from MXene.

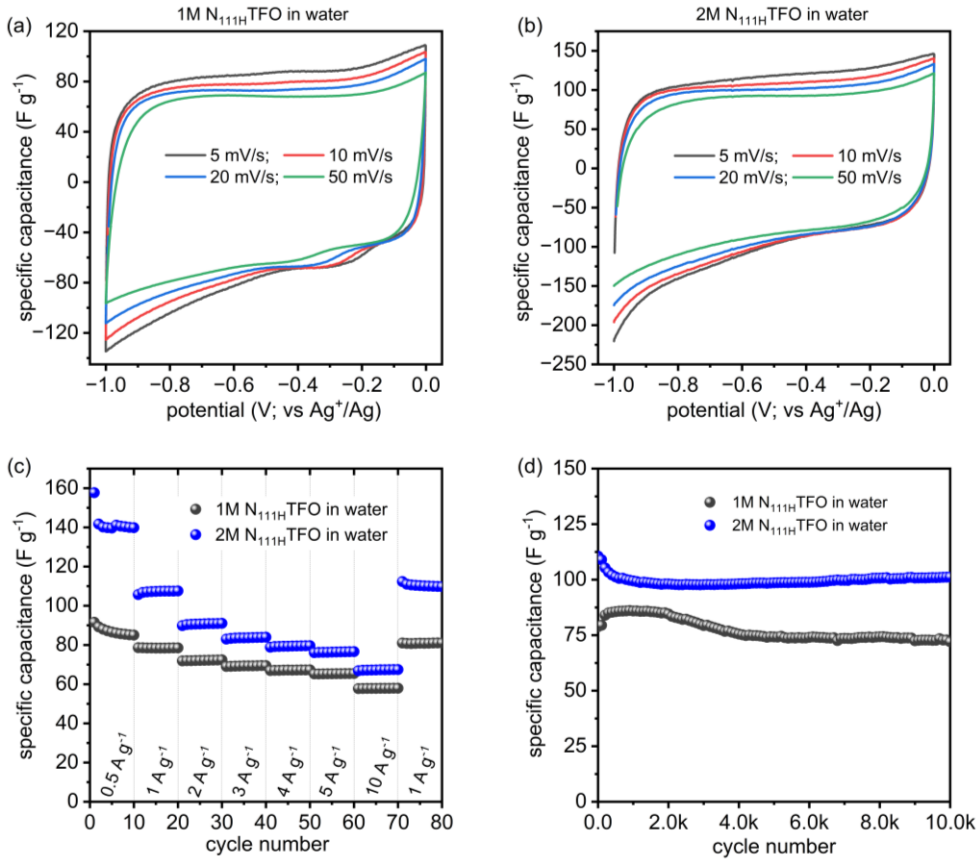

Figure 24. *(a-b) CV performance for protic IL in water at various sweep rates; (c) specific capacitance as a function of applied current density; and (d) cycling stability measured at 1 A/g.*

The rate performance of MXene electrodes was further assessed via GCD measurements at various current densities. **Figure 24c** show that specific capacitance increases with electrolyte concentration. The cell with 2M N111HTFO electrolyte delivered 107 F/g at current density of 1 A/g, compared to 78.5 F/g in the 1M solution. The enhanced performance is attributed to improved ion-transport at higher salt concentrations, aligning well with the conductivity results in **Figure 23a**. Further, cycling stability tests were performed at a current density of 1 A/g over 10,000 charge-discharge cycles (**Figure 24d**). The MXene electrode in 2M N111HTFO in water retained over 91% of its initial capacitance, while the 1 M system exhibited slightly lower retention under the same conditions. These results confirm that $Ti_3C_2T_x$ MXene exhibits excellent long-term electrochemical stability in protic IL-based electrolytes, highlighting its potential for reliable supercapacitor applications.

Following the promising half-cell performance of $Ti_3C_2T_x$ MXene electrodes, it was essential to evaluate their performance in a full-cell configuration. Accordingly, an asymmetric SC cell was constructed using $Ti_3C_2T_x$ MXene as the anode and activated carbon (AC) as the cathode and tested in 1M and 2M N111HTFO aqueous electrolytes. The performance of the MXene//AC full cells was assessed at two operating voltages, 0.7 V and 0.8 V, to examine the impact of applied voltage. CV curves recorded at 5 mV/s exhibited quasi-rectangular shapes for both electrolyte concentrations and voltages (**Figure 25a,d**), indicating EDLC behavior.

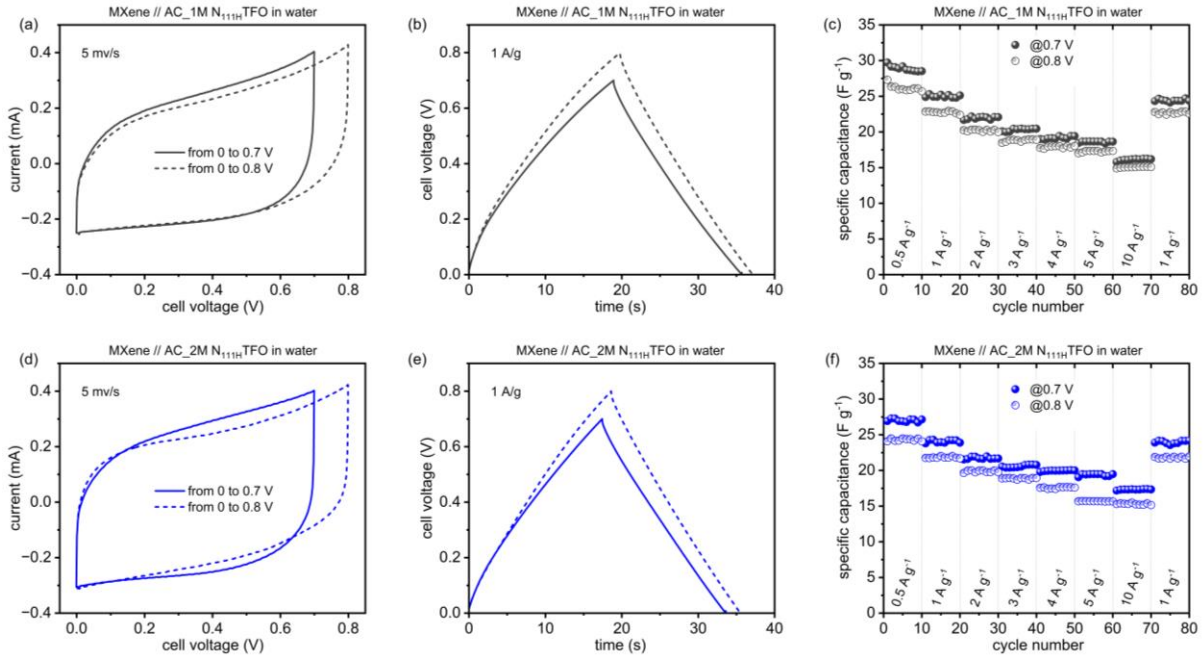

Figure 25. *Electrochemical performance of MXene // AC cell in a protic IL in aqueous electrolyte: (a-c) CV, charge-discharge and specific capacitance in 1M N_{111H}TFO; and (d-f) CV, charge-discharge and specific capacitance in 2M N_{111H}TFO.*

GCD curves (**Figure 25b,e**) revealed symmetric and nearly linear profiles in both 1M and 2M N_{111H}TFO electrolytes, confirming good capacitive behavior and electrochemical reversibility. While a slightly higher IR drop was observed at 0.8 V, due to increased voltage stress, it remained within operational limits. Specific capacitance values, calculated from GCD data at different current densities (**Figure 25c,f**), showed consistently better performance. Importantly, both systems demonstrated stable capacitance retention with increasing current densities, indicating good rate capability.

While 2M N_{111H}TFO in water clearly enhances MXene performance in half cells, the overall full-cell performance (MXene//AC) reflects the combined behavior of both electrodes. This may be due to AC does not benefit as much from increased electrolyte concentration, and hence the cell performance becomes similar in both 1M and 2M systems (**Figure 26a**). Further, to evaluate the long-term stability of the MXene//AC asymmetric cells, galvanostatic charge-discharge cycling tests were conducted over 10k cycles at a constant current density of 1A/g. As shown in **Figure 26b**, both 1M and 2M N_{111H}TFO-based cells exhibited excellent cycling stability, with minimal degradation in specific capacitance, confirming robust electrode behavior in both electrolyte concentrations. To gain deeper insight into the electrode/electrolyte interfacial characteristics, EIS measurements were performed before and after cycling, as presented in **Figure 26c-d**. The Nyquist plots indicate negligible changes in the key resistance parameters, including electrolyte resistance (R_e), charge transfer resistance (R_{ct}), and Warburg impedance. The preservation of these parameters over 10k cycles confirms the stable interfacial integrity and efficient ion transport pathways within the MXene//AC system.

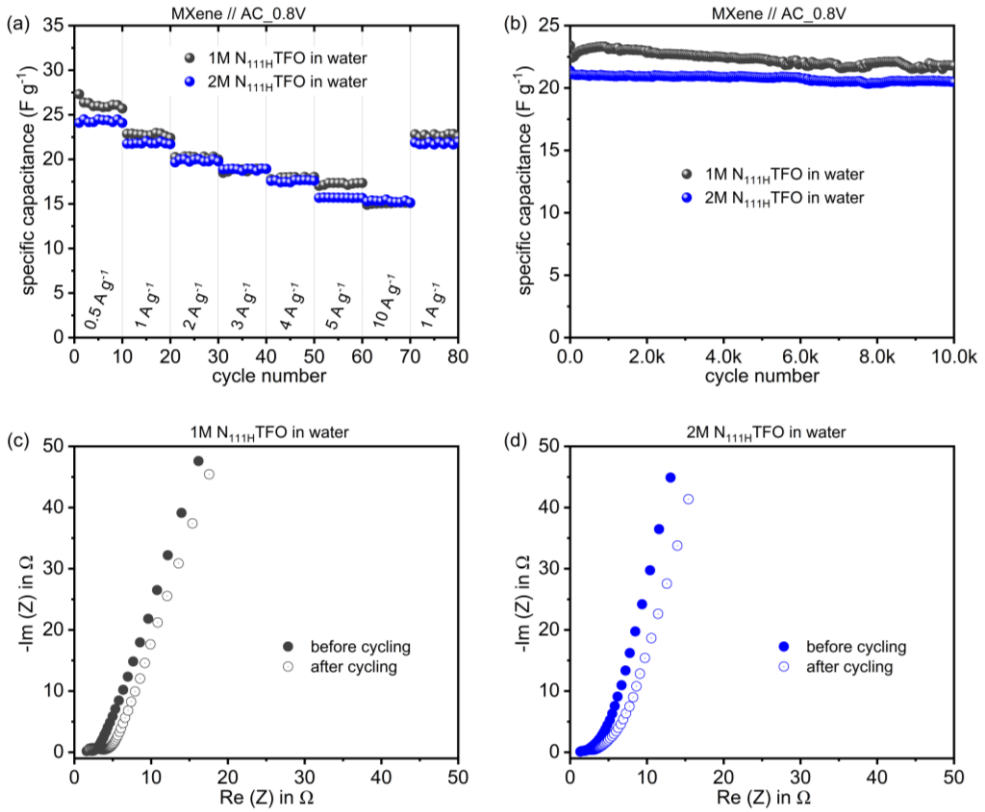

Figure 26. *(a) comparative specific capacitance of the MXene//AC cell; (b) cycling stability over 10k CD cycles; (c-d) electrochemical impedance spectra recorded before and after the stability test.*

Finally, the float test was conducted at a constant cell voltage of 0.8 V for both 1M and 2M N_{111H}TFO in water-based electrolytes. As illustrated in **Figure 27a**, the float test results demonstrate promising long-term stability, with both electrolyte systems maintaining stable capacitance over 1000 hours. MXene//AC cell in 2M N_{111H}TFO initially exhibited a slight drop in capacitance during the early stages of floating. However, the performance stabilized after few hours. Notably, the cell with 1M N_{111H}TFO displayed exceptional float performance, retaining over 91% of its initial capacitance after 1000 hours, indicating excellent electrochemical and structural stability under continuous voltage stress. EIS measurements before and after the float test (**Figure 27b-c**) support these observations. The Nyquist plots reveal only minimal changes in impedance parameters, in case of 1M electrolyte, indicates electrode/electrolyte interfaces remain unaffected by prolonged operation (**Figure 27b**).

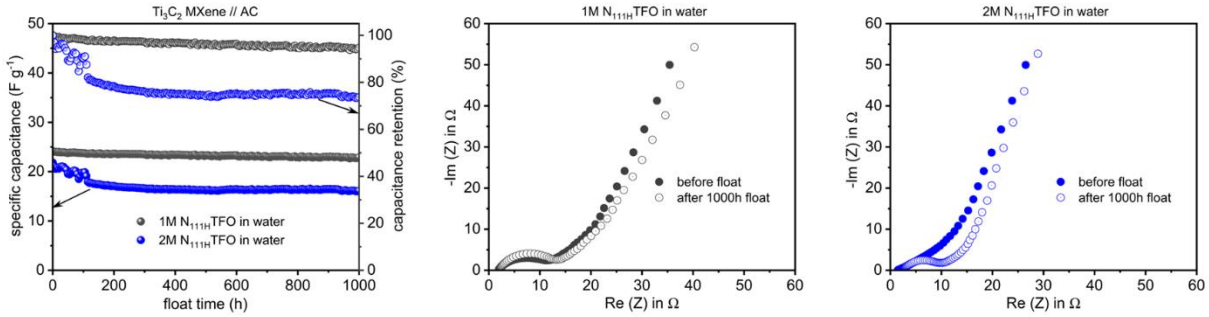

Figure 27. *float test of the MXene//AC cell at 0.8V and corresponding EI spectra recorded before and after 1000h of floating.*

In summary, the $Ti_3C_2T_x$ MXene electrode exhibits strong electrochemical performance in both half-cell and full-cell (MXene//AC) configurations when tested with the investigated protic IL electrolytes. Furthermore, the results highlight the excellent long-term stability of the MXene//AC cells, underscoring their potential candidates for SCs applications in protic IL systems.

At FSU, the electrochemical performance of $Ti_3C_2T_x$ MXene electrodes was also evaluated in 1M and 2M N_{111H}TFO dissolved in acetonitrile (ACN), using a three-electrode configuration. The results are summarized in **Figure 28**. CV measurements recorded at various scan rates showed quasi-rectangular shapes for both electrolyte concentrations, indicating typical capacitive behavior with major contribution from EDLCs (**Figure 28a-b**). The rate capability was assessed by GCD measurements at different current densities. Both concentrations displayed stable responses across the tested current densities (**Figure 28c**). The specific capacitance values obtained were approximately 30 F/g for the 1M solution and 24 F/g for the 2M solution. These values are lower compared to those observed in aqueous-based electrolytes. Additionally, cycling stability tests demonstrated consistent performance over 10k charge-discharge cycles (**Figure 28d**), highlighting the good stability of the MXene electrodes in organic media.

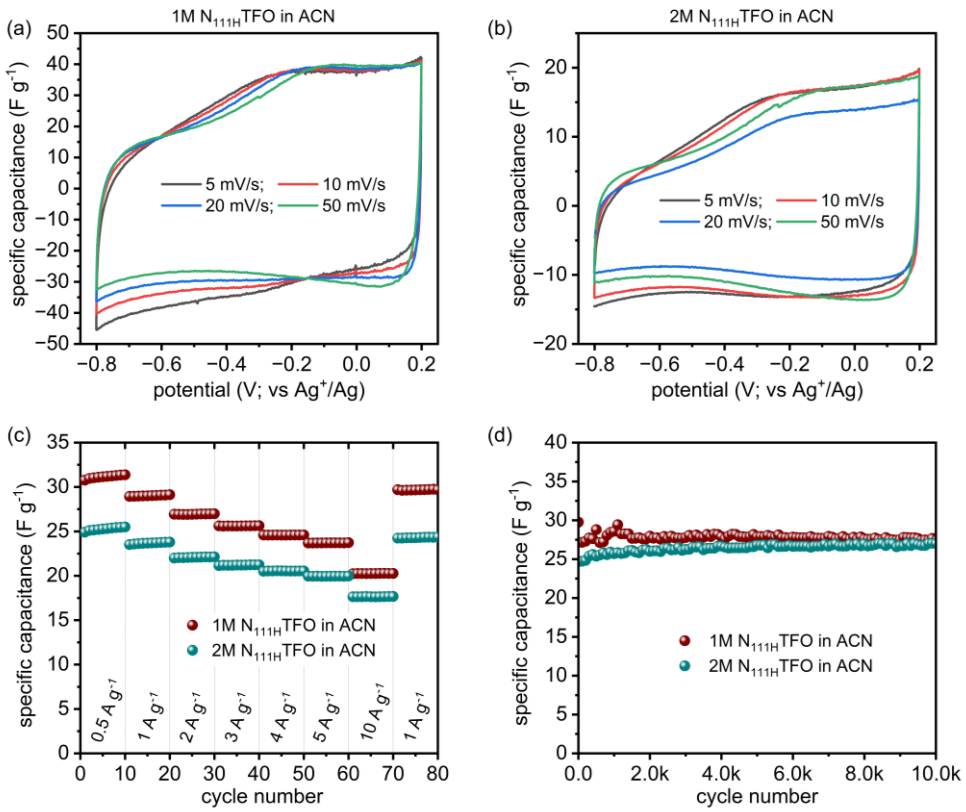

Figure 28. *(a-b) CV performance for protic IL in ACN at various sweep rates; (c) specific capacitance as a function of applied current density; and (d) cycling stability measured at 1 A/g.*

The lower capacitance in ACN-based systems may be attributed to factors such as differences in ion solvation dynamics, higher viscosity, and altered electrode/electrolyte interfacial behavior in organic solvents. These factors can hinder ion transport and reduce effective charge storage. However, the

system shows promise and could benefit from further optimization of electrolyte composition and electrode architecture to enhance performance.

3.1.3.6 Electrochemical characterisation of functionalized $Ti_3C_2T_x$ MXene

Electrochemical characterization of $Ti_3C_2T_x$ MXene functionalized with 5,5'-bis(triisopropoxysilyl)-2,2'-bipyridine (BPS) was performed by UNISTRA using $Ti_3C_2T_x$ MXene provided by TCD. The objective was to assess the impact of surface functionalization on the electrochemical performance of MXene-based electrodes for asymmetric supercapacitor applications. **Figures 29a** and **29b** show CV measurements carried out in a three-electrode configuration to determine the electrochemical stability window of the individual electrode materials. The working electrodes were pristine $Ti_3C_2T_x$, $Ti_3C_2T_x$-BPS, or activated carbon (AC), all deposited on carbon paper. An Ag/AgCl electrode served as the reference, and activated carbon was used as the counter electrode. The electrolyte was 1 M H_2SO_4. The CV curves for $Ti_3C_2T_x$ and $Ti_3C_2T_x$-BPS (**Figure 29a**) displayed stable capacitive behavior in the range of –0.4 to +0.3 V vs Ag/AgCl, beyond which current distortion indicated the onset of side reactions such as water decomposition. In contrast, the AC electrode (**Figure 29a-b**) maintained a much wider potential window, from –0.3 to +0.9 V vs Ag/AgCl, consistent with its excellent electrochemical stability. These measurements were used to define the operating voltage window (0-1.4 V) for the asymmetric supercapacitor cells used in subsequent two-electrode tests. **Figures 29c** and **29d** present CV curves of the assembled two-electrode asymmetric supercapacitors using $Ti_3C_2T_x$ or $Ti_3C_2T_x$-BPS as the negative electrode and AC as the positive electrode. Both devices showed quasi-rectangular CV profiles with minor distortions, indicating a combination of EDLC and pseudocapacitive behavior. Notably, the $Ti_3C_2T_x$-BPS//AC device exhibited larger current densities across all scan rates, confirming enhanced charge storage capability. The improvement is attributed to the presence of redox-active bipyridine groups in BPS and to improved ion transport enabled by the functionalization.

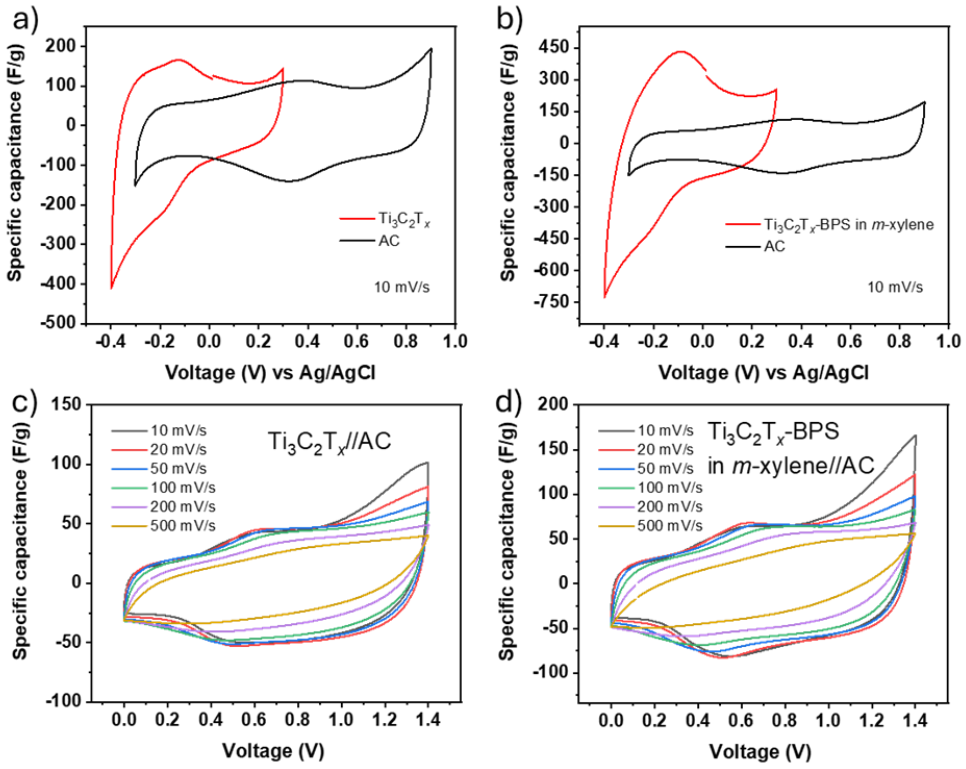

Figure 29. *CV curves of individual electrodes(a) pristine $Ti_3C_2T_x$, (b) $Ti_3C_2T_x$-BPS in m-xylene and AC, (c-d) CV curves at various scan rates of the corresponding devices.*

Figure 30 explores electrochemical kinetics and performance mechanisms in greater depth. The log(i) vs. log(scan rate) plots in **Figures 30a** and **30b** yielded b-values close to 1 for both devices (0.98 for $Ti_3C_2T_x$//AC and 0.96 for $Ti_3C_2T_x$-BPS//AC), indicating dominant capacitive behavior with minor diffusion-controlled contributions. **Figures 30c** and **30d** separate the total current into capacitive and diffusion-controlled components, showing that the BPS-functionalized system retained a strong capacitive character while introducing additional pseudocapacitive charge storage. At 10 mV/s, $Ti_3C_2T_x$-BPS exhibited 79% capacitive contribution versus 89% for pristine MXene. **Figures 30e** and **30f** visually represent these contributions, highlighting the higher overall current response of the functionalized electrode. Nyquist plots in **Figure 30g** reveal a lower solution resistance (0.35 Ω vs 1.53 Ω) for the BPS-functionalized system, indicating enhanced ionic conductivity. **Figure 30h** shows a steeper slope in the low-frequency region, reflecting improved proton diffusion, which nearly doubled (from 2.26×10^{-12} cm^2/s to 4.08×10^{-12} cm^2/s) after functionalization. Finally, **Figure 30i** and **Table 6** summarize key performance metrics in a radar plot, confirming that the BPS-functionalized $Ti_3C_2T_x$ significantly outperforms the pristine material in terms of ionic transport, pseudocapacitance, and porosity, while maintaining acceptable conductivity. These enhancements are attributed to the synergistic effects of covalent surface modification and structural optimization enabled by BPS, particularly when applied in *m*-xylene.

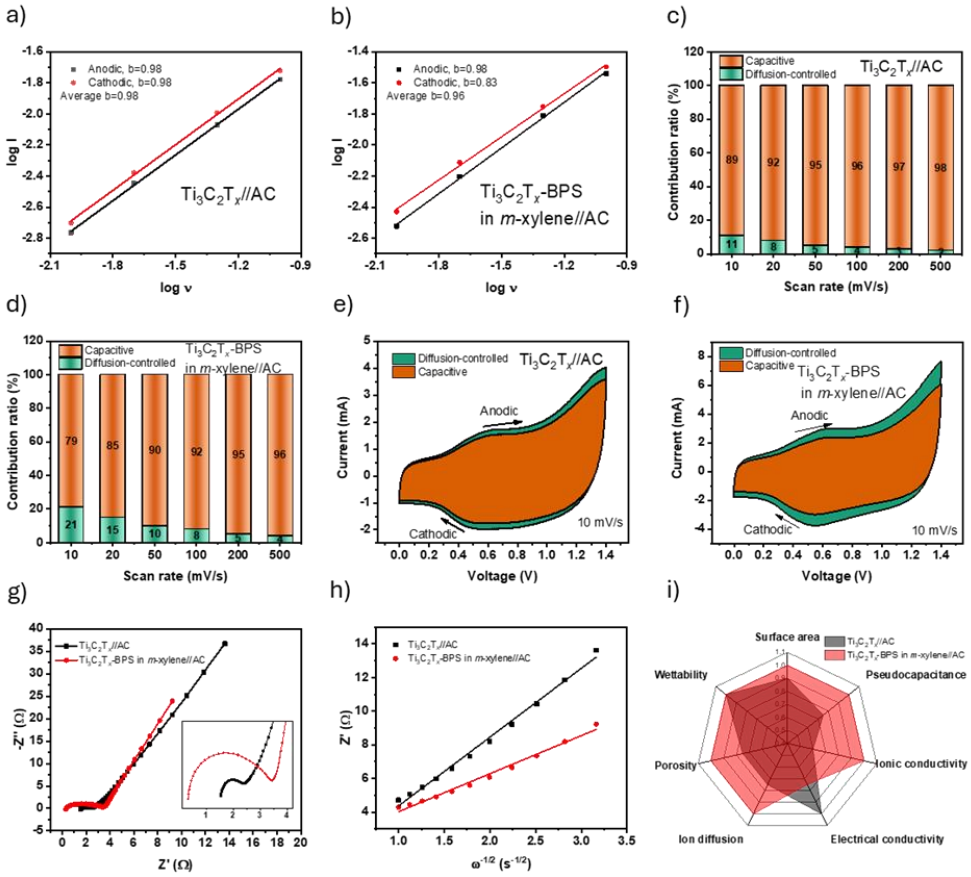

Figure 30. *Fitting plots between log(i) and log (ν) at various peak currents for (a) pristine $Ti_3C_2T_x$, and (b) $Ti_3C_2T_x$-BPS in m-xylene. Capacitive (contribution) and diffusion-controlled contribution of (c) $Ti_3C_2T_x$, and (d) $Ti_3C_2T_x$-BPS in m-xylene at various scan rates. Capacitive (contribution) and diffusion-controlled contribution fraction for the CV curve at 10 mV/s of (e) pristine $Ti_3C_2T_x$, and (f) $Ti_3C_2T_x$-BPS in m-xylene. (g) Nyquist plots of pristine $Ti_3C_2T_x$ (black curve), and $Ti_3C_2T_x$-BPS in m-xylene (red curve). (h) Corresponding linear relation between $\omega^{-1/2}$ and Z' in the low frequency region of the Nyquist plots of pristine $Ti_3C_2T_x$ (black curve), and $Ti_3C_2T_x$-BPS in m-xylene (red curve). (i) Radar chart comparing key electrochemical and structural performance metrics of pristine $Ti_3C_2T_x$ and $Ti_3C_2T_x$-BPS in m-xylene.*

Table 6. Physicochemical properties of pristine $Ti_3C_2T_x$ and $Ti_3C_2T_x$-BPS in *m*-xylene.

Property	**$Ti_3C_2T_x$**	**$Ti_3C_2T_x$-BPS in *m*-xylene**
Surface area	42.70 ± 0.54 m^2/g	47.06 ± 0.48 m^2/g
Porosity	Microporosity	Microporosity & mesoporosity
Pseudocapacitance	$Ti_3C_2T_x$	$Ti_3C_2T_x$ + BPS
Electrical conductivity	4766.98 S/cm	1956.08 S/cm
Ionic conductivity	0.59 mS/cm	2.95 mS/cm
Ion diffusion	2.26 10^{-12} cm^2/s	4.08 10^{-12} cm^2/s
Wettability	Highly hydrophilic	Highly hydrophilic

3.1.3.7 Electrochemical characterisation of hybrids composed of rGO or GO with $Ti_3C_2T_x$ MXene

UNISTRA performed the electrochemical characterization of pristine and hybrid materials by CV in three-electrode system, which consisted of: (*i*) a working electrode - pristine or hybrid material, (*ii*) a counter electrode - AC, (*iii*) a reference electrode - Ag/AgCl, and (*iv*) an electrolyte - 1M H_2SO_4. The measurements were conducted using various scan rates (5, 10, 20, 50, 100, and 200 mV/s).

Figure 31 shows the CV curves of rGO (a), $Ti_3C_2T_x$ MXene (b), and several hybrid combinations: rGO+$Ti_3C_2T_x$ (c), rGO+(3-aminopropyl)triethoxysilane (APTES) (d), $Ti_3C_2T_x$+APTES (e), and rGO+APTES+$Ti_3C_2T_x$ (f). The CV response of the rGO+$Ti_3C_2T_x$ hybrid (**Figure 31c**) exhibits a broader potential window compared to pristine rGO (**Figure 31a**), as it integrates the electrochemical range of both components. This hybrid also maintains a more rectangular shape at higher scan rates, indicating improved capacitive behavior and conductivity. The inclusion of APTES in the hybrids leads to subtle changes in the potential window. For example, rGO+APTES (**Figure 31d**) and $Ti_3C_2T_x$+APTES (**Figure 31e**) both show a slight extension of the window toward more positive potentials. However, in the $Ti_3C_2T_x$+APTES case, this gain is partially offset by a reduced stability in the negative potential range. The ternary hybrid rGO+APTES+$Ti_3C_2T_x$ (**Figure 31f**) successfully combines the potential windows of both rGO and $Ti_3C_2T_x$, achieving the broadest overall range among the tested materials.

Notably, the hybrid materials display CV curve shapes that resemble rGO at higher scan rates, which may indicate that rGO dominates the charge transport mechanism under fast cycling conditions. This suggests that rGO helps to stabilize the electrochemical response and supports rapid electron transfer within the hybrids. Capacitance values were calculated from the CV curves at 5 mV/s, yielding:

Electrode	**Capacitance (F/g)**
rGO	296.8
$Ti_3C_2T_x$ MXene	339.4
rGO+$Ti_3C_2T_x$	414.1
rGO+APTES	269.3
$Ti_3C_2T_x$+APTES	418.2
rGO+APTES+$Ti_3C_2T_x$	390.5

These results confirm that combining rGO and $Ti_3C_2T_x$ enhances capacitive performance. The highest capacitance was observed for the $Ti_3C_2T_x$+APTES hybrid, closely followed by the rGO+$Ti_3C_2T_x$ and rGO+APTES+$Ti_3C_2T_x$ materials, indicating that appropriate functionalization and hybridization strategies can significantly boost energy storage performance.

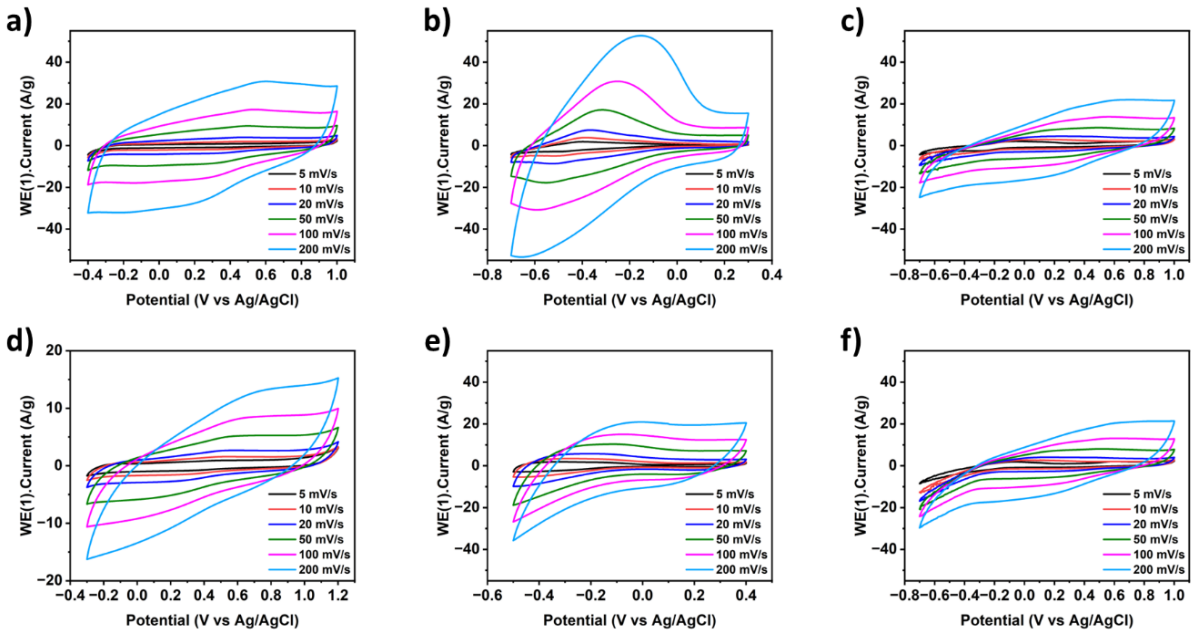

Figure 31. *CV curves at various scan rates of: (a) rGO, (b) $Ti_3C_2T_x$ MXene, (c) rGO+$Ti_3C_2T_x$ MXene stirring 24h, (d) rGO+APTES, (e) $Ti_3C_2T_x$+APTES, and (f) rGO+APTES+$Ti_3C_2T_x$ in the three-electrode system.*

To further assess the electrochemical behavior of the rGO/$Ti_3C_2T_x$ hybrids under more practical conditions, symmetric two-electrode coin cells were assembled using 3M H_2SO_4 as the electrolyte. **Figure 32** presents the CV curves of the individual components, rGO (**Figure 32a**) and $Ti_3C_2T_x$ MXene (**Figure 32b**), as well as two rGO+$Ti_3C_2T_x$ hybrids prepared by different methods: mechanical grinding (**Figure 32c**) and stirring for 24 hours (**Figure 32d**). The measurements were performed at scan rates ranging from 10 to 200 mV/s. Compared to the individual materials, the hybrid electrodes showed significantly enhanced electrochemical performance. At a scan rate of 10 mV/s, the calculated specific capacitances were:

Electrode	**Capacitance (F/g)**
rGO	92.0
$Ti_3C_2T_x$ MXene	48.7
rGO+$Ti_3C_2T_x$ (grinded)	166.4
rGO+$Ti_3C_2T_x$ (stirred 24h)	191.6

These results indicate that hybridization substantially improves charge storage capability. The sample prepared by 24-hour stirring exhibited the highest capacitance, suggesting better dispersion and interfacial contact between rGO and $Ti_3C_2T_x$, which likely facilitated more efficient ion transport and charge accumulation. The quasi-rectangular CV shapes of the hybrids, especially at higher scan rates, confirm their capacitive behavior and suggest improved electrochemical kinetics compared to the pristine components.

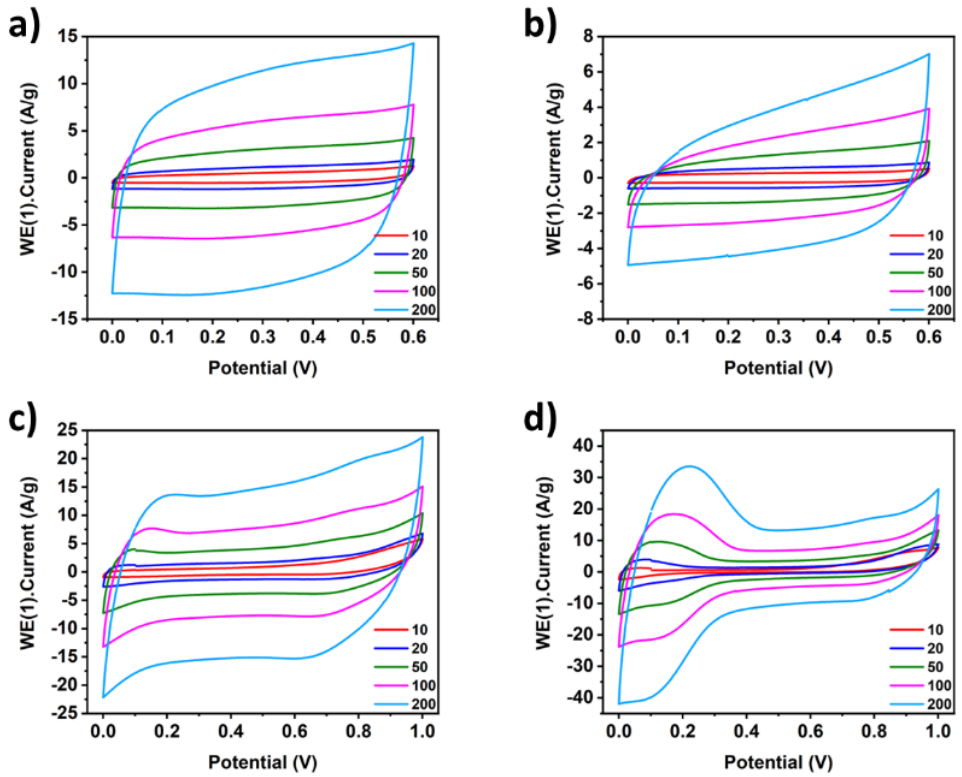

Figure 32. *CV curves at the different scan rates: (a) rGO; (b) $Ti_3C_2T_x$ MXene; (c) rGO+$Ti_3C_2T_x$ hybrid grinded; (d) rGO+$Ti_3C_2T_x$ hybrid stirring 24 hours in the two-electrode system.*

To investigate the impact of thermal treatment and GO-based hybridization on electrochemical performance, CV measurements were conducted in a three-electrode system for a series of GO-based composites. **Figure 33** displays the CV curves at various scan rates for: GO+APTES, thermally treated GO+APTES (140 °C, 5h), GO+APTES+$Ti_3C_2T_x$, and thermally treated GO+APTES+$Ti_3C_2T_x$. All materials were evaluated in 1M H_2SO_4 using Ag/AgCl as the reference electrode and activated carbon as the counter electrode.

Across all four samples, the potential windows were relatively similar, showing no significant extension compared to rGO-based materials. However, the overall current responses, and consequently, the capacitance values, were significantly lower. This highlights the inferior conductivity and electrochemical activity of GO compared to rGO, likely due to the lack of a continuous conductive network in the former.

At a scan rate of 5 mV/s, the GO+APTES composite exhibited a very low capacitance of only 9.9 F/g (**Figure 33a**). Upon thermal treatment at 140 °C for 5 hours, this increased to 36.7 F/g (**Figure 33b**), indicating partial restoration of conductivity and improved interaction between the functional groups. For the GO+APTES+$Ti_3C_2T_x$ hybrid, the capacitance reached 84.5 F/g (**Figure 33c**), while the thermally treated version achieved a much higher value of 186.6 F/g (**Figure 33d**). Although thermal annealing clearly enhanced electrochemical performance, these values still remained substantially lower than those achieved with rGO-based hybrids (e.g., over 400 F/g), underscoring the critical role of conductive carbon frameworks in optimizing charge transport and maximizing capacitance.

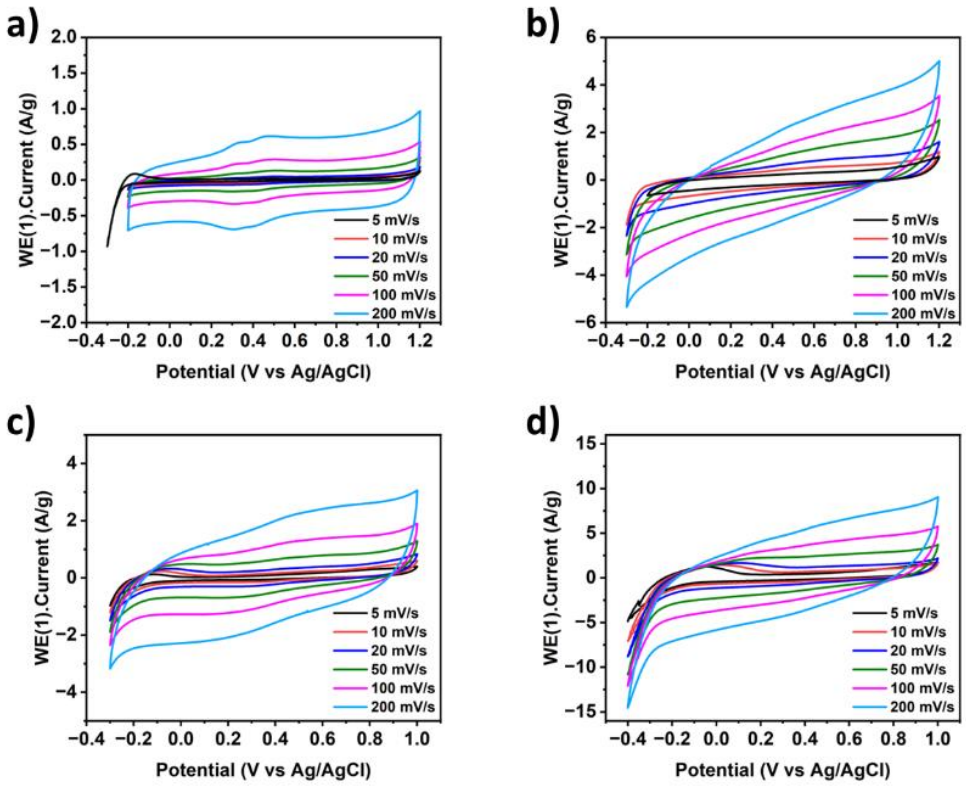

Figure 33. *CV curves at various scan rates of: (a) GO+APTES; (b) GO+APTES 140°C, 5h; (c) GO+APTES +$Ti_3C_2T_x$, (d) GO+APTES +$Ti_3C_2T_x$ 140°C, 5h in the three-electrode system.*

Figure 34 compares the capacitance values of various pristine and hybrid materials as a function of scan rate, evaluated in both three-electrode (**Figure 34a-c**) and symmetric two-electrode (**Figure 34d**) systems. In the three-electrode configuration, **Figure 34a** shows the performance of rGO, $Ti_3C_2T_x$ MXene, and their direct hybrids. Among these, the rGO+$Ti_3C_2T_x$ hybrid prepared by 24-hour stirring exhibited the highest capacitance (414.1 F/g at 5 mV/s), followed closely by the $Ti_3C_2T_x$+APTES hybrid (418.2 F/g), shown in **Figure 34b**. **Figure 34c** presents the comparison of GO-based hybrids before and after thermal treatment. As expected, thermal annealing significantly improved the capacitance, particularly for the GO+APTES+$Ti_3C_2T_x$ composite. Despite these high initial values, the hybrid materials exhibited a more rapid decline in capacitance as the scan rate increased, compared to the pristine rGO or $Ti_3C_2T_x$. This performance drop at higher scan rates may be attributed to factors such as material degradation, restacking, or increased resistance, possibly due to partial oxidation in the aqueous H_2SO_4 electrolyte. These findings suggest that while hybridization enhances low-rate performance, electrochemical stability at high rates could benefit from further optimization, potentially through the use of organic electrolytes to mitigate oxidation and improve long-term integrity.

Figure 34d summarizes the capacitance trends in the two-electrode system, which is more representative of practical device configurations. Although the overall capacitance values in this setup are significantly lower than those in the three-electrode system, the hybrids (particularly rGO+$Ti_3C_2T_x$, stirred for 24h) still outperform the pristine materials. Importantly, the capacitance of all materials remained relatively stable across increasing scan rates, indicating improved electrochemical robustness and rate capability in the full-cell configuration. This highlights a key trade-off: while

absolute capacitance is reduced, performance consistency is better preserved in the two-electrode system.

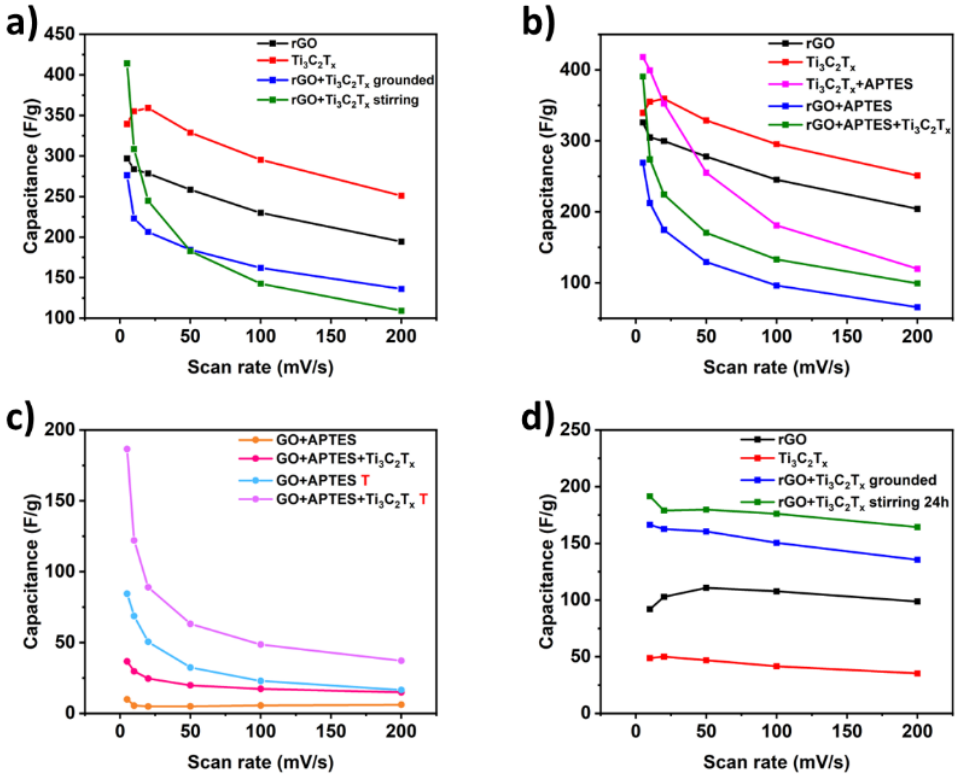

Figure 34. *Comparison of capacitance in the three-electrode system at different scan rates: (a) rGO, $Ti_3C_2T_x$ MXene, and their hybrids; (b) rGO, $Ti_3C_2T_x$ MXene, and their hybrids with APTES; (c) GO+APTES and GO+APTES+$Ti_3C_2T_x$ before and after heating at 140°C, 5h. (d) Comparison of capacitance in the symmetric two-electrode system at different scan rates rGO, $Ti_3C_2T_x$ MXene, and their hybrids.*

3.1.3.8 Electrochemical characterisation of CG and $Ti_3C_2T_x$ MXene hybrids

In addition, UNISTRA carried out electrochemical studies on new hybrid systems composed of $Ti_3C_2T_x$ and Mo_2C MXenes (both provided by TCD) combined with curved graphene (CG, supplied by SKL). Similar to the previously studied rGO+$Ti_3C_2T_x$ hybrids, these systems aimed to synergize the high electrical conductivity and ion transport of MXenes with the structural stability and accessible surface area of CG. The goal was to enhance both performance and cycling stability in supercapacitor applications.

CV measurements were conducted in a symmetric two-electrode configuration using 3M H_2SO_4 as the electrolyte. The materials evaluated included the individual components, CG, $Ti_3C_2T_x$, and Mo_2C, as well as their 1:1 mass-ratio hybrids: CG+$Ti_3C_2T_x$ and CG+Mo_2C. The CV curves for the CG+Mo_2C hybrid (**Figure 35c**) display features from both individual components, with the broad rectangular profile of CG (**Figure 35a**) and the pseudocapacitive response of Mo_2C (**Figure 35b**). However, despite the initially higher current, the final capacitance of CG+Mo_2C drops to nearly the same level as CG alone (**Figure 35f**), indicating limited synergy and suggesting that the two components are not well-matched. For the CG+$Ti_3C_2T_x$ hybrid (**Figure 35e**), performance was even more limited. Although $Ti_3C_2T_x$ alone showed a

moderate capacitance (**Figure 35d**), the hybrid exhibited a significant drop in performance, with capacitance values approaching zero at higher scan rates (**Figure 35f**). This outcome indicates poor electrochemical compatibility between CG and $Ti_3C_2T_x$ under the tested conditions. The poor performance of both hybrids can be attributed to several factors: possible restacking of layers, blockage of MXene active sites by CG, unoptimized mass ratios, or insufficient interfacial contact. Furthermore, the use of an aqueous electrolyte may lead to oxidation of MXene surfaces, further impairing performance. These results suggest that for CG-MXene hybrids to be effective, further optimization is needed. This includes adjusting the CG:MXene ratio to promote better synergy, and considering alternative (e.g., organic) electrolytes to preserve the structural and electrochemical integrity of MXenes during operation.

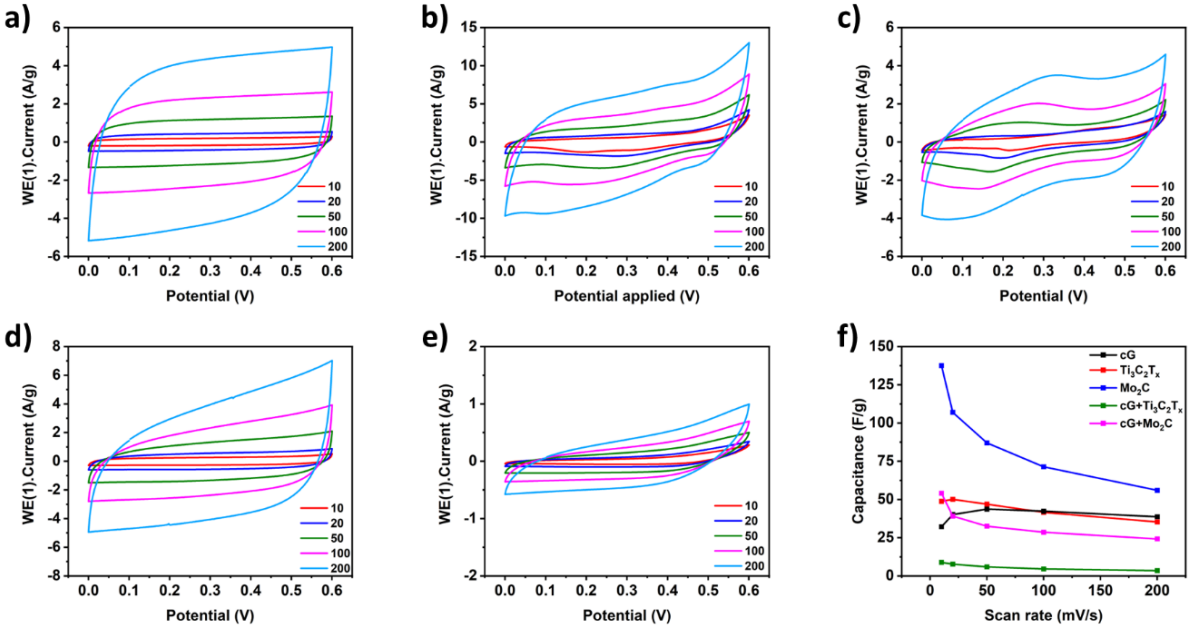

Figure 35. *CV curves in two-electrode system at different scan rates: (a) CG; (b) Mo_2C MXene; (c) CG+Mo_2C; (d) $Ti_3C_2T_x$ MXene; (e) CG+ $Ti_3C_2T_x$. (f) Comparison of performance of initial and hybrid materials based on CV measurements at different scan rates.*

3.2 Contribution to project (linked) Objectives

This deliverable directly contributes to multiple key objectives of the GREENCAP project, as outlined in the Description of Action (DoA) Part B on pages 5 and 6.
By advancing the development of scalable, CRM-free, and environmentally sustainable materials for supercapacitors (SCs), the efforts in this deliverable support GREENCAP's overarching goals to produce high-performance energy storage devices that adhere to sustainable manufacturing standards.

Specific contributions to project objectives are as follows:

a. The deliverable reports significant progress toward the objective of creating CRM-free electrode materials and electrolytes. Several innovative materials and methods have been developed:
   - Few-Layer Graphene (FLG) production has been optimized to replace N-Methyl-2-pyrrolidone (NMP) with water-based, non-toxic media and surfactants, significantly enhancing the sustainability of FLG synthesis by eliminating harmful solvents.
   - Synthetic Graphite Exfoliation via electrochemical methods has been refined, enabling high-yield production of few-layer graphene from synthetic, non-CRM sources. This innovation reduces reliance on natural graphite, a critical raw material, further supporting CRM-free production objectives.
   - CRM-Free MXenes have been synthesized successfully using both mild etching and molten-salt methods, providing a range of materials that can serve as high-performance electrode materials without relying on CRMs.

b. Several key advancements in the formulation of electrolytes and electrode materials contribute to enhanced energy storage and efficiency for SCs:

   - Aprotic ILs have been formulated specifically for EDLCs, where selected IL candidates show promising potential to boost energy storage capacity.

   - Protic ILs have been developed for MXene-based electrodes, with initial trials showing favorable electrochemical performances.

These electrolyte and EM innovations contribute to GREENCAP's objective of maximizing SC performance. By refining the electrochemical interactions between materials, the project enhances the energy density, charge/discharge efficiency, and longevity of SCs, thus directly addressing the goal of advancing high-performance energy storage solutions.

3.3 Contribution to major project exploitable result

This deliverable contributes significantly to reaching several of the project targets and exploitable results defined in the GREENCAP project. The developments outlined in this deliverable offer both scientific discoveries and new designs, along with potential products and processes that can be exploited commercially or used to inform future developments in the field of SCs.

Specific contributions include:

3.3.1 Exploitable Results: New Products (Electrode Materials and Electrolytes)

- **CRM-Free Electrode Materials:**

- The successful development of CRM-free MXenes and CG using sustainable, green methods contributes to the creation of novel electrode materials. These materials can be exploited for the development of high-performance SCs, addressing both environmental and performance-related concerns in energy storage applications.

- **IL-Based Electrolytes:**
  - Protic and aprotic ionic liquids (ILs) have been developed for use with MXenes, CG and other electrode materials. These ILs have shown promising electrochemical performance and can be used to further enhance the energy density and efficiency of supercapacitors. The research has identified the best-performing IL candidates, which can be exploited for use in next-generation SCs, offering improved safety, stability and performance.

3.3.2 Exploitable Results: New Processes (Sustainable and Scalable Manufacturing Methods)

- The refined synthesis processes for CG and MXenes**,** represent new, scalable processes for producing high-quality, sustainable materials for SCs. These processes utilize water-based solvents and mild etching techniques, significantly reducing environmental impact by eliminating the need for toxic solvents (e.g., NMP).
- The work on scalable production at rates of approximately 1 kg per day positions these processes as industrially viable, paving the way for large-scale manufacturing of CRM-free supercapacitors.
- Developing the ILs discussed herein on Solvionic's pilot line is allowing Solvionic to improve the yield, output and scalability of IL electrolytes

3.3.3 Exploitable Results: Scientific Discovery (Improved Electrochemical Performance)

- The deliverable includes the discovery of new IL formulations that improve the performance of supercapacitors, specifically in terms of energy storage capacity, cycle stability, and efficiency. The development of IL-functionalized MXenes holds great potential for further scientific exploration into improving the electrochemical properties of electrode materials.

3.3.4 Exploitable Results: New Designs (Materials and Manufacturing Techniques for SCs)

- The development of novel electrode materials, such as CRM-free MXenes and CG, along with tailored electrolyte formulations, represents a significant advancement toward more efficient and sustainable supercapacitor technologies. These innovations support scalable manufacturing processes and are well-suited for deployment across a broad range of energy storage applications in various industries.

- The integration of high-conductivity materials, both protic and aprotic ILs, and innovative electrode architectures enables the design of supercapacitors with improved charge storage capabilities and faster charge/discharge performance, addressing key performance demands in modern energy systems.

4 Conclusion and Recommendation

This deliverable provides a detailed electrochemical assessment of electrode/electrolyte interfaces relevant to next-generation SCs systems. 1M $N_{1113}FSI$ in ACN was assessed as the first-generation (GEN1) electrolyte. However, accelerated ageing tests conducted by industrial level in cylindrical cells (WP4) revealed degradation under floating conditions. In response to these findings, 1M $Pyr_{11}BF_4$ and 1M $Pyr_{13}BF_4$ in ACN were formulated as GEN2 candidates and are currently under evaluation for improved thermal and electrochemical stability. The outcomes of this work contribute directly to goals of developing sustainable, CRM-free energy storage technologies, while also providing a robust platform for further scientific development, commercial scaling, and potential input into policy frameworks supporting green innovation and energy transition.

5 Risks and interconnections

5.1 Risks/problems encountered

No risk to report.

5.2 Interconnections with other deliverables

This derivable is closely interconnected with Deliverable D1.2 and D2.2

6 Deviations from Annex 1

No deviations to report.

7 References

1) Patil, I. M., Burton, T., Ladam, A., Fantini, S., and Balducci, A., Electrochemical performance of electrochemical double layer capacitors containing pyrrolidinium and ammonium fluorosulfonyl imide in acetonitrile-based electrolytes. *Electrochimica Acta*, **2025**, *525*, 146133.

2) Gamberini, A., Burton, T., Ladam, A., Bagheri, A., Abruzzese, M., Beydaghi, H., ... and Bellani, S., Ionogel-Based Electrodes for Non-Flammable High-Temperature Operating Electrochemical Double-Layer Capacitors. *ChemSusChem*, **2025**, *18*(10), e202401874.

3) Rongying, L. I. N., Falgayrat, A., Aravena, C., Fantini, S., & Malbosc, F., Method and apparatus for making electrodes for an ionic liquid-based supercapacitor, and method for making such a supercapacitor, *U.S. Patent No. 12,142,426*. Washington, DC: U.S. Patent and Trademark Office.

8 Acknowledgement

The author(s) would like to thank the partners in the project for their valuable comments on previous drafts and for performing the review.

Project partners:

#	Partner short name	Partner Full Name
1	BED	BEDIMENSIONAL SPA
2	SOLV	SOLVIONIC
3	FSU	FRIEDRICH-SCHILLER-UNIVERSITAT JENA
4	SKL	SKELETON TECHNOLOGIES OU
5	TCD	THE PROVOST, FELLOWS, FOUNDATION SCHOLARS & THE OTHER MEMBERS OF BOARD, OF THE COLLEGE OF THE HOLY & UNDIVIDED TRINITY OF QUEEN ELIZABETH NEAR DUBLIN
6	TUD	TECHNISCHE UNIVERSITAET DRESDEN
7	UNISTRA	UNIVERSITE DE STRASBOURG
8	SM	SKELETON MATERIALS GMBH
9	UNR	UNIRESEARCH BV
10	CNR	CONSIGLIO NAZIONALE DELLE RICERCHE
11	UCAM	THE CHANCELLOR MASTERS AND SCHOLARS OF THE UNIVERSITY OF CAMBRIDGE
12	CU	Y CARBON LLC

This project has received funding from the European Union's Horizon Europe research and innovation programme under grant agreement No 101091572. Views and opinions expressed are however those of the author(s) only and do not necessarily reflect those of the European Union. Neither the European Union nor the granting authority can be held responsible for them.

9 Appendix A - Quality Assurance Review Form

The following questions should be answered by all reviewers (WP Leader, reviewer, Project Coordinator) as part of the Quality Assurance procedure. Questions answered with NO should be motivated. The deliverable author will update the draft based on the comments. When all reviewers have answered all questions with YES, only then can the Deliverable be submitted to the EC.

NOTE: This Quality Assurance form will be removed from Deliverables with dissemination level "Public" before publication.

Question	WP Leader	Reviewer	Project Coordinator
	Artur Ciesielski (UNISTRA)	Valeria Nicolosi (TCD)	Francesco Bonaccorso (BED)
1. *Do you accept this Deliverable as it is?*	Yes	Yes	Yes
2. *Is the Deliverable complete?* - *All required chapters?* - *Use of relevant templates?*	Yes	Yes	Yes
3. *Does the Deliverable correspond to the DoA?* - *All relevant actions preformed and reported?*	Yes	Yes	Yes
4. *Is the Deliverable in line with the GREENCAP objectives?* - *WP objectives* - *Task Objectives*	Yes	Yes	Yes
5. *Is the technical quality sufficient?* - *Inputs and assumptions correct/clear?* - *Data, calculations, and motivations correct/clear?* - *Outputs and conclusions correct/clear?*	Yes	Yes	Yes
6. *Is created and potential IP identified and are protection measures in place?*	Yes	Yes	Yes
7. *Is the Risk Procedure followed and reported?*	Yes	Yes	Yes
8. *Is the reporting quality sufficient?* - *Clear language* - *Clear argumentation* - *Consistency* - *Structure*	Yes	Yes	Yes